Lake Champlain Basin Program

TECHNICAL REPORT NO. 102

Quantifying Phosphorus Retention in Restored Riparian Wetlands of the Lake Champlain Basin

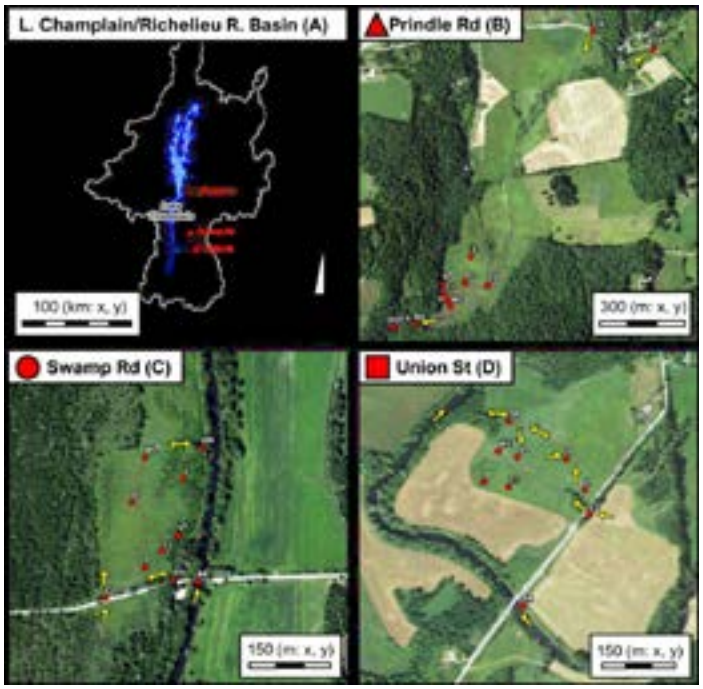

March 2022

Prepared by:
Eric D. Roy University of Vermont

For:
The Lake Champlain Basin Program and
New England Interstate Water Pollution Control Commission

This report was funded and prepared under the authority of the Lake Champlain Special Designation Act of 1990, P.L. 101-596 and subsequent reauthorization in 2002 as the Daniel Patrick Moynihan Lake Champlain Basin Program Act, H. R. 1070, through the US EPA. Publication of this report does not signify that the contents necessarily reflect the views of the states of New York and Vermont, the Lake Champlain Basin Program, or the US EPA.

The Lake Champlain Basin Program has funded more than 100 technical reports and research studies since 1991. For complete list of LCBP Reports please visit:
https://www.lcbp.org/news-and-media/publications/technical-reports/

NEIWPCC Job Code: 995-002-001

QUANTIFYING PHOSPHORUS RETENTION IN RESTORED RIPARIAN WETLANDS OF THE LAKE CHAMPLAIN BASIN

Lake Champlain Basin Program Final Project Report

NEIWPCC Job Code: 995-002-001
Project Code: LS-2018-026
Contractor: University of Vermont
Prepared By: Eric D. Roy
Date Submitted: December 21, 2021
Date Approved: March 28, 2022

CONTACT INFORMATION
Eric D. Roy
University of Vermont, 81 Carrigan Dr., Burlington, VT 05405
Phone: 802-656-7359
Fax: 802-656-8683
eroy4@uvm.edu

This project was selected for funding by the Lake Champlain Basin Program (LCBP) Steering Committee and it has been supported directly by an agreement or sub-award issued by NEIWPCC. NEIWPCC manages LCBP's personnel, contracts, grants, and budget tasks through a partnership with the LCBP Steering Committee.

Although the information in this document may have been funded wholly or in part by the United States Environmental Protection Agency (under agreement CE982720010), the National Park Service, or by the International Great Lakes Fishery Commission, through their respective contracts to NEIWPCC, it has not undergone review by the Agency, Service, or Commission, and no official endorsement of the content of the document should be inferred. The viewpoints expressed here do not necessarily represent those of NEIWPCC, the LCBP, the USEPA, the NPS, or the GLFC, nor does mention of trade names, commercial products, or causes constitute endorsement or recommendation for use.

Suggested Citation:
Roy, E.D., A.R.H. Wiegman, W.B. Bowden, and K. Underwood. 2021. "Quantifying phosphorus retention in restored riparian wetlands of the Lake Champlain Basin." Report to the Lake Champlain Basin Program, March 28, 2022

Executive Summary

The State of Vermont and non-profit organizations are pursuing nature-based solutions to help meet reductions in phosphorus (P) loads to Lake Champlain required by the US EPA's total maximum daily load (TMDL). One such nature-based solution is the restoration of riparian wetland ecosystems. Within the Lake Champlain Basin (LCB), most potential riparian wetland restoration sites were formerly used for agriculture. While the capacity for wetlands to serve as nutrient sinks has been established generally, very few studies have examined net P retention for the specific case of restored riparian wetlands on historically drained and farmed land, with no such studies in the Northeast U.S. We fill this important knowledge gap using a combination of field studies for three restored riparian wetlands in the LCB (2019-2021), laboratory measurements and experiments, and process-based modeling. The three field sites were located in the Otter Creek (2) and Lewis Creek (1) watersheds. We directly quantified numerous wetland P stocks and fluxes during this project, including water quality monitoring during three flood pulses at each site. These measurements, combined with information available in peer-reviewed literature and other concurrent studies in Vermont, established a foundation for process-based P modeling to determine net P retention incorporating both particulate and dissolved P dynamics.

Our results, using a newly coded Wetland P Model in R, indicate that particulate P deposition and dissolved P loss are both important in determining net P retention. Across model scenarios using what we consider the most realistic assumptions, net P retention in restored wetlands was approximately 0.1 g P m^{-2} yr^{-1} (1 lb P $acre^{-1}$ yr^{-1}). Very few scenarios resulted in net P export, suggesting that the wetlands investigated in this study are generally P sinks on the landscape. If foregone P loading from former agricultural land use is also factored in, the overall net P load reduction benefit of conversion of agricultural land to wetland could increase to 0.2 or 0.3 g P m^{-2} yr^{-1} (2 or 3 lbs P $acre^{-1}$ yr^{-1}). The modeled wetland retention efficiencies for total P (TP) and soluble reactive P (SRP) were on average +38% (net gain) and -23% (net loss), respectively, but varied widely across all site-scenario combinations, illustrating the importance of site factors (e.g., equilibrium P concentration for soils), hydrology, and influent total suspended solids (TSS) and TP concentrations. These results highlight the potential TP load reduction benefits associated with the restoration of floodplain wetlands. However, they also suggest that release of legacy P in soluble forms can potentially complicate watershed management efforts. Wetland net P retention in modeled scenarios was positively related to upstream concentrations of TSS and P. Therefore, if upstream watershed management efforts effectively reduce riverine TSS and P concentrations, the net P retention benefits of riparian wetlands will likely decrease, with more legacy P released as SRP to floodwaters. For example, net P retention values ranged from <0 to 0.08 g P m^{-2} yr^{-1} (<0 to 0.7 lbs P $acre^{-1}$ yr^{-1}) and 0.1 to 0.3 g P m^{-2} yr^{-1} (0.9 to 2.7 lbs P $acre^{-1}$ yr^{-1}) for 0.5x median stream concentrations and 2x median stream concentrations, respectively.

In conclusion, this project has addressed important gaps in understanding the extent to which restored riparian wetlands will serve as a P sink in the LCB, corresponding to Strategies I.A.1.c (Increase understanding of factors affecting BMP performance and efficiency) and I.C.1.b (Fund programs to protect or enhance river corridors for nutrient reduction and flood resilience) within the LCBP 2017 Opportunities for Action. Outputs from this project can aid the refinement of wetland restoration efforts, resulting in efficient use of state and non-profit resources to reduce P loading to Lake Champlain.

1. Project Synopsis

The State of Vermont and non-profit organizations are pursuing nature-based solutions (Albert et al., 2017) to help meet reductions in phosphorus (P) loads to Lake Champlain required by the US EPA's total maximum daily load (TMDL) (US EPA, 2016). This includes the restoration of wetlands in the Lake Champlain Basin (LCB). More than 4,000 potential wetland restoration sites in Vermont have been ranked using a GIS-based prioritization model, which will inform future efforts (VT DEC, 2018; Arrowwood, 2017). Nevertheless, there remains a lack of field data demonstrating the extent to which restored riparian wetlands will serve as a P sink generally (Hoffmann et al., 2009), and especially in the LCB. This project addressed this information gap, which falls under Strategies I.A.1.c (Increase understanding of factors affecting BMP performance and efficiency) and I.C.1.b (Fund programs to protect or enhance river corridors for nutrient reduction and flood resilience) within the LCBP 2017 Opportunities for Action. Outputs from this project will aid the refinement of wetland restoration efforts, resulting in efficient use of state and non-profit resources to reduce P loading to Lake Champlain.

Generalizations about the P retention efficacy of wetlands are difficult to make, especially for restored riparian wetlands (Land et al., 2016; Fisher & Acreman, 2004; Currie et al., 2017). Some studies of restored riparian wetlands report net P retention driven by particulate P deposition, while others have found potential for P export (Hoffmann et al., 2009; Jones et al., 2015), or decreasing P retention over time (Mitsch et al., 2012). P retention in wetlands occurs due to settling and trapping of P associated with particles, chemical reactions with iron (Fe), aluminum (Al), calcium (Ca), and magnesium (Mg), and accretion of P-containing organic matter (Reddy et al., 1999). P can be exported from wetlands as soluble reactive P (SRP) due to release of legacy P in soils, exhaustion of soil P sorption capacity, and the decomposition of organic matter (Reddy et al., 1999). In riparian wetlands, P retention is strongly linked to local hydrology, which influences P loading rate, sedimentation, contact between water and soil/sediments, P uptake by vegetation, and decomposition (Hoffmann et al., 2009). Vegetation type and landscape characteristics (e.g., soils, prior land use) are also key drivers of riparian wetland P dynamics (Kiedrzyńska et al., 2008; Figure 1).

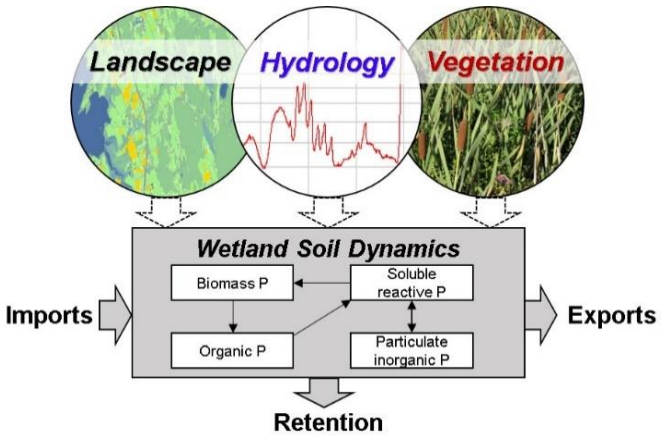

Figure 1. Hydrology, landscape, and vegetation interact to influence wetland phosphorus (P) dynamics. These factors ultimately control P inputs to restored riparian wetlands, P retention within restored riparian wetlands, and export of P from restored riparian wetlands.

The overarching aim of this project was to provide a systematic assessment of P dynamics, including P deposition, internal P cycling, and P release as SRP, in selected restored riparian wetlands within the LCB using a combination of modeling and field studies. Our specific objectives were:

> **Objective 1. Initial Model Development** - Enhance and parameterize existing process-based models to simulate the hydrology and P dynamics (e.g. settling, mineralization, and vegetation uptake) of selected restored riparian wetlands.
>
> **Objective 2. Field Studies** - Field assessment of P storages and dynamics in 15 plots across three restored riparian wetlands, including inundation events.
>
> **Objective 3. Model Calibration and Scenarios** - Assessment of model simulations to determine potential for short-term and long-term P retention effectiveness for selected restored riparian wetlands under various scenarios.

For this LCBP project, we focused our efforts on three restored riparian wetland sites that were formerly drained and used for agricultural production. We measured numerous P stocks, P fluxes, and P transformations at these three sites to enhance our understanding of factors that influence net P retention during flood inundation events and to inform our modeling task. This included field monitoring of three flood inundation events at each site. Additionally, we were able to supplement data collected at these three sites as part of this LCBP-funded project with data resulting from separate research efforts by project team members spanning a larger number of riparian sites in Vermont, as well as available literature data, allowing us to better contextualize our LCBP project findings. Throughout this report, we clearly demarcate LCBP project data versus external data sources.

This project benefitted from multiple partnerships. The Vermont Chapter of The Nature Conservancy (TNC) and the USDA Natural Resources Conservation Service Vermont facilitated site access and provided information on land use history and restoration actions. The Vermont DEC Wetlands Program assisted the project team on separate wetland soils research that we use in this report to contextualize our findings. The UVM Gund Institute for Environment provided financial support for graduate student Adrian Wiegman, who played a critical role in all project tasks as part of his PhD dissertation research. The Rubenstein School of Environment and Natural Resources supported the PI as project cost share. Undergraduate students were able to participate in the project through awards provided by the Gund Institute for Environment and the UVM Office of Fellowships, Opportunities, & Undergraduate Research.

2. Tasks Completed

We identified four tasks necessary to fulfill our project objectives (Table 1). For the first task, we developed a Quality Assurance Project Plan (QAPP), which was approved in February 2019, with amendments to the document in October 2019 and July 2021. The remaining three tasks are associated with the three project objectives as described below.

Table 1. Project tasks and deliverables.

Task #	Task Title	Objective	Deliverable or Output	Timeline
1	Develop a QAPP	Describe quality assurance procedures that will maintain project performance.	QAPP Approval	February 2019
2	Initial Model Development	Enhance and parameterize existing process-based models to simulate the hydrology and P dynamics (e.g. settling, mineralization, and vegetation uptake) of selected restored riparian wetlands.	Parameterized (but not calibrated) process-based model, including sensitivity analysis.	February-December 2019
3	Field Studies	Field assessment of P storages and dynamics in 15 plots across three restored riparian wetlands, including inundation events.	Detailed description of results for P storages and dynamics.	February 2019-October 2021
4	Model Calibration and Scenarios	Assessment of model simulations to determine potential for short-term and long-term P retention effectiveness for selected restored riparian wetlands under various scenarios.	Calibrated model and description of results for simulations.	January-December 2021
5	Approved quarterly reports	Report activities each quarter	Approved quarterly reports	January 2019 – December 2021
6	Approved final report	Compile project summary, results, model documentation, and other project materials (e.g., photographs).	Approved final report	December 30, 2021

2.1. Initial Model Development

Initial model development proceeded as planned, resulting in the creation of a new Wetland P Model coded in R version 4.0.1. This model was informed by past models described in the literature and designed specifically to determine wetland net P balance as a function of both particulate and dissolved P fluxes.

2.2. Field Studies

We quantified numerous P stocks and fluxes in three restored riparian wetland sites within the LCB during 2019-2021, resulting in detailed information on soil P fractions, potential for SRP

release from soils during inundation, and cycling of P associated with organic matter (e.g., P in plant biomass and litter). This also included hydrologic and water quality monitoring for three flood inundation pulse events per site. Field studies included 5 plots per site corresponding to elevation quintiles. This approach allowed us to quantify trends in P deposition across elevation gradients and yielded data that informed model calibration and sensitivity analysis.

2.3. Model Calibration & Scenarios

We calibrated the Wetland P Model using the first year of field data along with literature values. We then performed verification using a second year of field data. Calibration/verification results were deemed satisfactory. We then conducted a wide-ranging sensitivity analysis that serves to examine net P retention under various realistic scenarios. This approach yielded a number of important insights on how site factors (e.g., equilibrium P concentration for soils), hydrology, and influent water quality influence net P retention.

3. Methodology

3.1. Initial Model Development

We coded and parameterized a Wetland P Model derived from existing process-based models (e.g., Wang and Mitsch, 2000; Hantush et al., 2013) in R version 4.0.1 to simulate the hydrology and P dynamics (e.g. settling, mineralization, and vegetation uptake) of selected restored riparian wetlands. The model described by Wang and Mitsch (2000) is a detailed and widely cited nutrient cycling model. WetQual, the model described by Hantush et al. (2013) is supported by the EPA and contains subroutines to simulate dissolved P flux. Our modeling objective was to simulate time series of different P pools at the plot-scale (i.e., establish the plot as the control volume) and then use the model to simulate a range of scenarios involving wetland-scale changes (i.e., external forcings) to estimate the magnitude of perturbation necessary for influencing P retention and exports at the plot scale. Modeling was achieved using mass balance modules for P (**P-module**) and water (**hydrology-module**).

The **P-module** simulates P fluxes and transformations in an aboveground floodwater layer as well as a single active soils layer. P retention and export rates are determined by representing changes in the mass balance of P, as follows:

$$\Delta P_{Total} = \Delta P_{soil} + \Delta P_{biomass} + \Delta SRP \qquad \text{(Eqn. 1)}$$

where P_{total} is total P (g P m^{-2}), P_{soil} is soil P (organic and inorganic particles), $P_{biomass}$ is aboveground and belowground plant biomass P, and SRP is soluble reactive P (i.e., dissolved inorganic P) in surface floodwater and soil porewater. Net changes in P_{soil} represent changes in soil particulate inorganic P and particulate organic P, which can occur due to sedimentation or erosion during inundation. Changes in soil particulate inorganic P depend on sorption/desorption rates that quantify P movement between the particulate inorganic P and SRP pools. In addition to sedimentation and erosion, soil organic P changes also reflect mineralization, which is the conversion of organic P to inorganic P during the decomposition of organic matter. Change in plant biomass P represents the balance of plant growth (and associated P assimilation) and senescence (transfer of P to litter pool), and was modeled as a function of air temperature, plant species, and nutrient availability (Wang & Mitsch, 2000). Change in SRP is a function of import

and export in floodwaters, mineralization, and flux between the soil porewater and water column (Hantush et al., 2013; Kalin et al., 2013).

River discharge and P concentration data are essential for estimating the percentage of the river P load that a wetland receives and retains over a given period and characterizing hydrologically driven changes to the wetland P mass balance. A **hydrology-module** was developed that characterizes P retention and export in riparian wetlands using: (i) relationships between depth and storage volume in both the water column and the active soil layer, (ii) relationships between water level and hydraulic residence time determined using previously developed models and our field measurements, (iii) wetland P concentrations in the water column and soil, (iv) P mass fluxes into and out of study control volumes, (v) meteorological observations from nearby stations, (vi) water temperatures and dissolved oxygen concentrations necessary for adjusting P transformation rates, and (vii) plant community characteristics. While many hydrologic inputs have a sub-daily temporal resolution, some P mass balance components were only assessed at weekly to monthly or seasonal timescales. Therefore, model performance was evaluated at multiple timescales.

The **hydrology-module** estimates the wetland outflow during a given time period $Q_{out,t}$ based on inflow volume (Q_{in}), precipitation ($Precip_t$), evapotranspiration (ET_t), and changes in wetland storage volume (ΔS_t) in both the water column and active soil layer:

$$Q_{out,t} = Q_{in,t} + (Precip_t - ET_t) - \Delta S_t \quad \text{(Eqn. 2)}$$

Q_{in} consists of surface flows informed by field measurements. Surface water outflows and the net groundwater exchange between the wetland and river are lumped into a deduced outflow term Q_{out}. Only surface-groundwater exchanges between the water column and active soil layer within the wetland were explicitly modeled because other groundwater exchanges typically comprise small fractions of water budgets of riparian wetlands underlain with low-permeability soils (Lent et al., 1997; Jones et al., 2015).

Next, the total outflow and export of P from the wetland (P_{out}) was estimated from river inputs (P_{in}) and changes in the wetland P mass:

$$P_{out,t} = P_{in,t} - \Delta P_{Total} \quad \text{(Eqn. 3)}$$

The P export from the wetland can also be computed as follows:

$$P_{out,t} = C_t Q_{out,t} \quad \text{(Eqn. 4)}$$

where C_t, the average P concentration in wetland surface water, is calculated as follows:

$$C_t = \frac{C_{t-1}S_{t-1} + C_{in}Q_{in} - C_{t-1}Q_{out}}{S_{t-1} + Q_{in} - Q_{out} + Precip_t - ET_t} \quad \text{(Eqn. 5)}$$

3.2. Field Studies

3.2.1. Study Areas

We studied three historically farmed wetlands in the Vermont portion of the Lake Champlain Basin (Figure 2). The study sites occupy two riparian settings that are typical for potential wetland restoration candidates with a history of farming in the region.

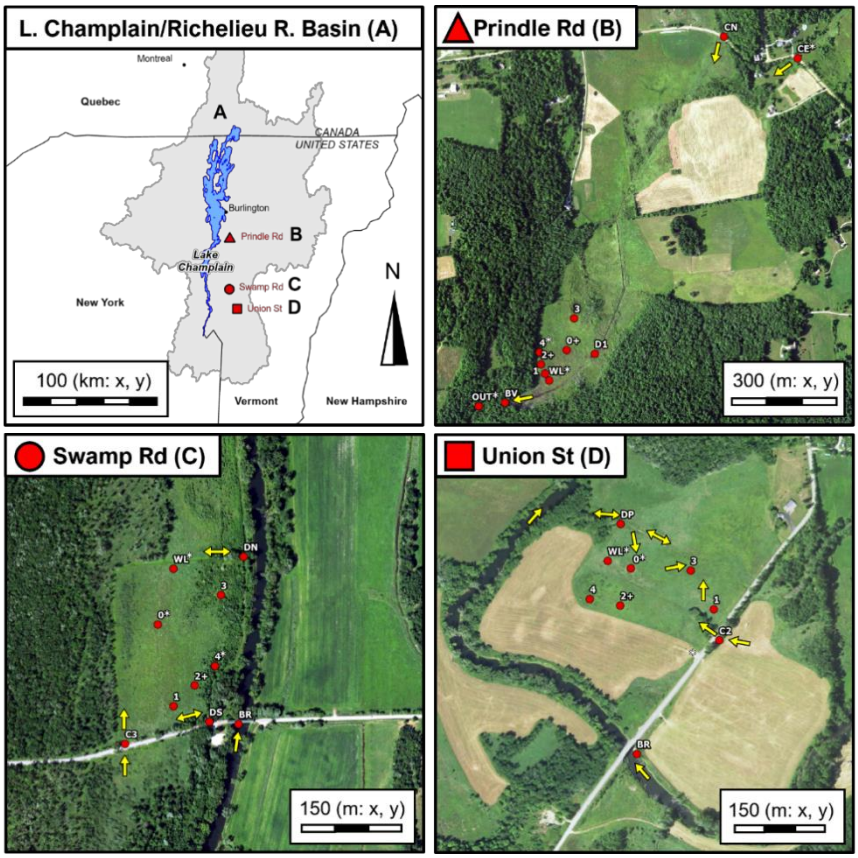

Figure 2. Map of the Lake Champlain and Richelieu River basin (A, Grey Area) showing sampling plot locations at each of the three study sites at Prindle Road (B), Swamp Road (C), Union Street (D). Yellow arrows indicate observed water flow directions. USDA national areal imagery color imagery from 2016; Plot label key: 0-4 = soil and vegetation sampling plots, C = culvert, D = drainage ditch, BR = bridge, + denotes locations of ISCO 4712 automatic water samplers and miniDOT dissolved oxygen and temperature loggers, * denotes locations of HOBO MX2100 water level logger.

One site was located along Prindle Brook, a small tributary of Lewis Creek near Prindle Road in the Town of Charlotte at Lewis Creek Hill Preserve owned by The Nature Conservancy (**Prindle Road** henceforth). Prindle Road (Figure 2b) is a headwater depression wetland that receives inflow from two first order streams from the northeast at two culverts that pass under Prindle Road. The site is underlain by a clay pan soil (NRCS hydrologic group D) and drains to a beaver dam near an outcropping of bedrock in the southwest. The catchment upstream of the Prindle Road site is a 2.5 km^2 area of low intensity development, and low to moderate intensity agriculture. The stream channel of Prindle Brook had been ditched and straightened to improve agriculture use in the 1960 and 1970s. By 2006 the agricultural activity within the sampling zone had stopped. Since then, hemlock trees were planted and large woody debris was placed in the drainage ditch. By 2018, the

first year we gained access to the site, beavers had recolonized the site and created a dam with a height of ~2 m above the eroded stream bed.

The two other sites are located along Otter Creek, which is the longest river draining to Lake Champlain in Vermont. One is located north of Swamp Road and west of Otter Creek in the Town of West Salisbury at Otter Creek Swamps Preserve, owned by The Nature Conservancy (**Swamp Road** henceforth). The Swamp Road site (Figure 2c) is located adjacent to mature scrub/shrub and bottomland hardwood forest to the west. Row crops, hayfields and concentrated dairy feeding operations lay across the river to the east. Nearly every year, floodwaters overtop the pavement along Swamp Road and a series of seven culverts were placed along the road to south and west of the site. Plans for hydrologic restoration that included ditch plugging were considered by TNC at this site, but ultimately never carried out due to concerns over increased flooding impacts and damages on Swamp Road. Despite this, accumulation of sediment and woody debris within the ditch may slow water drainage from the site relative to when it was an active farm field (>10 years ago). The other Otter Creek site is north of Union Street and east of Otter Creek in the Town of Brandon on an NRCS wetland reserve easement (**Union Street** henceforth). The study site at Union Street (Figure 2d) is in a low area along the inside of a river bend that is traversed by Union Street. The study area was ditched and farmed conventionally as early as 1942, but by the late 1990s the site was used as a hay field and by 2004 the sampling zone was no longer being farmed, though an adjacent higher elevation zone was being used for organic hay with cow manure application every 2-3 years between 2004 and 2017. In 2018, an armored earthen plug was placed in the ditch connecting the wetland to the river and an artificial meander scar and berm near the outfall of a culvert was excavated to promote wildlife habitat. In 2019, volunteer groups planted native tree species at high elevation zones within the site. The ditch plug raised the height of the ditch by about 3 feet so that the site now retains water even after the river drops below the bottom of the ditch.

The Otter Creek sites are positioned 25 km apart along an un-dammed reach of well-connected floodplain wetlands that was once intensively ditched, logged and farmed. Otter Creek has drainage areas of 1210 km^2 and 1410 km^2 at the Union Street and Swamp Road bridges, respectively (Ries et al., 2017). Streamflows in this section of Otter Creek are gauged upstream at Rutland, VT (USGS gauge no. 0428000) and downstream at Middlebury, VT (USGS gauge no. 0428500). Over the past 20 years many agricultural fields along this reach have been retired, and in some areas the floodplain forest is regenerating. Currently, much of this reach of Otter Creek is protected under conservation easement, through the Natural Resources Conservation Service (NRCS) Wetland Reserve Program. As the Otter Creek flows from upstream to downstream, the wetland complex attenuates a large amount of floodwater, helping to reduce flow peaks downstream. As a result, the downstream river gauge at Middlebury is characterized by flood pulses of smaller amplitude but longer duration when compared to the gauge upstream of the floodplain complex in Rutland (Trueheart, et al., 2020; Watson, et al., 2016). The section of Otter Creek near Swamp Road is characterized by annual flooding that ranges from weeks to months during the wet seasons (October through May). The floodplain at Union Street is narrower and flood peaks are higher but shorter compared to the Swamp Road downstream site. Both sites show patterns of flow through ditches that reverse when the floodplain is filling or draining relative to the river.

We delineated a sampling zone polygon within each site that had uniform prior land use and perennial emergent vegetation based on available areal imagery in Google Earth Pro. We then removed areas from each sampling zone that were not likely to receive floodwater at least once during the 2-yr monitoring campaign. At the two Otter Creek sites, the sampling zone was clipped with a polygon of the maximum inundation extent for the spring flood of 2018 (which was roughly a ~Q1.5-year flood). The aforementioned polygon was produced by a 2D HEC-RAS model (Trueheart et al., 2020) of the Otter Creek floodplain between Rutland and Middlebury, and was verified in the field in 2018 by examining the predicted flooding depth against the high water mark on trees. At Prindle Road, we did not have a model to estimate the maximum flooding extent, so we collected GPS points of the flooding extend during the spring flood in May of 2019, and adjusted the sampling zone not to exceed the elevation of the high water mark.

We distributed 5 circular plots (5m radius) within each sampling zone along an elevation gradient based on 0.7m resolution LiDAR elevation data (VGCI 2018). This was done by reclassifying the sampling zone at each site into five equal area pentile groups based on elevation, with each group accounting for 20 percent of the area inside the sampling zone. One sampling plot was randomly placed within each pentile. We also set up additional sampling plots for taking water samples from the river upstream of each site and at ditches and other likely water flow paths during flooding and draining. Inset maps for each study site including sampling plots and instrument locations are provided in Figure 2.

3.2.2. Soil Analyses

In July of 2019, duplicate soil samples (surficial 0-5 and 5-10cm, excluding surface litter) were collected from each plot in each study site using 7-cm diameter polycarbonate coring tubes, transported to the lab in a cooler, and then stored at 4°C until processing. At the lab, 20-30g subsamples of each soil sample were analyzed for gravimetric moisture content by drying at 60°C (Reddy, et al. 2013), and additional subsamples were air-dried (25°C) for certain protocols. Dried subsamples were then sieved (<2mm) and homogenized, and a subsample was ground with a mortar and pestle. Dried, processed soils were sealed in water-tight polypropylene containers and stored in the dark at room temperature until further analysis.

Within the first week of sample collection, we initiated a sequential P fractionation that separates five operational fractions of soil P (Reddy et al. 1998; Roy et al. 2017) using 1-2 g field-moist soil samples: (1) readily available P [20 mL 2 M KCl extraction for 1h, analyzed for SRP], (2) Fe/Al-bound Pi [20 mL 0.1 M NaOH extraction for 17h, analyzed for SRP], (3) alkali extractable Po [= 0.1 M NaOH TP – 0.1 M NaOH-Pi], (4) Ca/Mg-bound Pi [20 mL 0.5 M HCl extraction for 24 h, analyzed for SRP] and (5) residual P [nitric acid digestion on residue from step 4, analyzed on ICP, Perkin-Elmer Avio 200 ICP-OES #0790004)] (Richardson & Reddy, 2013). We calculated total P (frac-TP) as the sum of all five fractions, Organic P (frac-P_o) as the sum of fractions 3 and 5, and inorganic P (frac-P_i) as the sum of fractions 1, 2, and 4 (Figure 3).

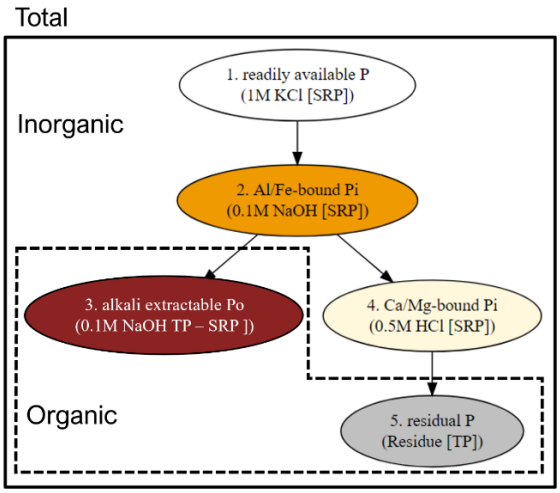

Figure 3. Flow diagram of sequential P fractionation showing inorganic and organic pools.

We also conducted a three-pool parallel fractionation for total, inorganic, and organic P (Levy & Schlesinger, 1999; Richardson & Reddy, 2013). For total P (HCl-TP), 0.3 g dried and ground soil subsamples were placed into pre-weighed borosilicate glass 15ml conical bottom extraction tubes then ashed and reweighed to estimate organic content via loss on ignition (LOI, at 550°C for 4 hours). Ashed samples were then extracted with 15 mL (1:50 m/v) of 1M HCl for 16 hrs. For inorganic P (1 M HCl-P_i), 0.3 g dried and ground soil subsamples were placed in HDPE centrifuge tubes and extracted in the same fashion as for 1M HCl-TP. Organic P (1 M HCl-P_o) was calculated as the difference between 1M HCl-TP and 1M HCl-P_i.

We determined oxalate-extractable forms of Al, Fe, Mn, and P (Al-ox, Fe-ox, Mn-ox, P-ox, respectively) by extracting air dried soil samples, 2mm sieved and ground, with acid ammonium oxalate for 3hrs in the dark following Courchesne & Turmel (2008). We diluted the extracts 5x in 0.1M nitric acid before analysis by ICP. With data from the oxalate extraction, we calculated the molar ratio of extractable elements (P to Al, P to Fe, and Al to Fe), P saturation ratio (PSR, molar ratio of P to the sum of Al and Fe), and soil P storage capacity (SPSC). SPSC was calculated following methods described by Nair & Harris (2004) using a P saturation ratio threshold of 0.23, which we determined for Vermont riparian soils as part of another project. Total minerals, including P, Fe, Al, Ca, Mg were determined using nitric acid microwave digestion following EPA method 3051 and analysis by ICP (abbreviations: P-3051a, Fe-3051a, etc.). Particle size analysis was run on air-dried and 2mm-sieved soils after overnight dispersion in Calgon solution. Clay was determined by the hydrometer method (Bouyoucos, 1962; Day, 1965). Sand was determined gravimetrically by wet sieving to <53µm (sieve No. 270). Silt was calculated as the remainder. Particle sizes and texture class are from the USDA Soil Survey Manual (Soil Science Division Staff, 2017).

3.2.2. Diffusion of SRP from Soils during Inundation

SRP flux is governed by sorption-desorption dynamics within the soil and the SRP concentration gradient between soil porewater and the overlying water column. Diffusive SRP flux between wetland soils and the overlying water column was estimated using an intact core method (Roy et al., 2012). First, 6 intact cores (7 cm dia., ~25 cm in length) were collected from the low, average, and high elevation plots at each site, sealed with rubber stoppers on the bottom and top and transported upright immediately to the lab. In the lab, any standing water was siphoned off and

then cores were carefully refilled to minimize sediment disruption with filtered (Whatman no. 2) site river water to 20 cm above the soil surface. All cores were divided into aerobic (3 per plot) and anaerobic treatments (3 per plot) and placed in a water bath to maintain stable temperature (20-25°C) within black tubs covered with blackout cloth to exclude light. Cores were sealed at the top with no. 12.5 two-hole rubber stoppers to regulate the flow of gas. For anaerobic incubations, O_2-free nitrogen gas was bubbled into the water column to purge all oxygen from the core for 24hr initially and then 1-2hr per day thereafter, and stopper holes were sealed when purging was not occurring. For the aerobic incubation, room air was bubbled into the water columns for 24hr initially and then 1-2hr per day thereafter, and stopper holes cores were unsealed throughout the experiment to allow air exchange. In the cores retrieved from the average elevation plot, we monitored temperature, dissolved oxygen, pH, specific conductivity, and oxidation reduction potential each day prior to sampling with a YSI Professional Plus. In the cores retrieved from the high and low elevation plots, only dissolved oxygen was measured each day, to confirm O_2 presence/absence. Water column samples (5mL) were collected ~5cm below the water surface repeatedly over the course of ~14d incubations, filtered (0.45 µm membrane filters), stored frozen, and analyzed for SRP using a microplate reader (BioTek Synergy HT) following the malachite green method for colorimetric orthophosphate analysis (D'Angelo et al. 2001; Ringuet et al. 2011). Within the cores, we maintained a 20 cm water column height at all times by adding additional filtered river water as needed via a syringe. The protocol we used to estimate diffusion of SRP from soils during inundation in this project is identical to the one used at other Vermont riparian locations as part of separate research efforts. Therefore, we are able to compare the flux rates observed at the three LCBP project sites to those for a broader group of sites (n = 20 plots in total, including LCBP project plots) in this report.

Within one week of collection from the field, we extracted moist soils for water extractable P (WEP) [2g dry equivalent of field-moist soil in 20 mL DDI H_2O extraction for 1h, analyzed for SRP]. To better characterize P sorption dynamics within our site soils, we used batch incubations to determine phosphate sorption isotherms following Graetz & Nair (2009). Briefly air-dried and sieved soils were composited volumetrically at each plot and depth, then ~1g aliquots of soil were equilibrated for 24hrs in the dark at 4°C in 20 mL of 0.01M KCl solution with concentrations (C) of phosphate as KH_2PO_4: 0, 0.1, 0.5, 0.1, 1, 10, 75 mg P L^{-1}. The amount of sorbed P (S) is calculated from the difference in concentration before and after each incubation. The initially sorbed P (S_0) was determined as the y-intercept parameter to a linear regression fit of S and C, at values of C below 1 mg P L^{-1}. The equilibrium P concentration where net sorption and desorption equal zero (EPC_0) was determined by solving for y equals zero using the linear regression fit for S and C, at values of C below 1 mg L^{-1}. A nonlinear Langmuir model was used to determine the bond energy (K_L) and maximum P sorption (S_{max}) for the S-C relationship using all concentrations (Bolster & Hornberger, 2007).

3.2.3. Vegetation Biomass

In early September 2019, aboveground biomass of herbaceous plants (macrophytes) was collected from triplicate 0.5m x 0.5m quadrats by clipping vegetation 1-2 cm above the soil or water surface (Dunne et al., 2007). At the same time, belowground biomass was collected in each herbaceous sampling quadrat by collecting the top 10cm of soil with a 7-cm diameter core tube. Biomass samples were placed in a cooler for transport and stored at 4°C until processing, which occurred within 1 month of sample collection. Belowground biomass samples were wet sieved with tap

water through a 1mm mesh to remove soil from roots and then dried at 60°C until constant weight (Dunne et al., 2007). In July 2021, diameter at breast height and at 30 cm was measured for trees and shrubs respectively, if woody biomass was present in a plot, then TP stocks were estimated non-destructively using literature values for P content and allometric equations. Aboveground herbaceous biomass samples were clipped into 10cm pieces dried and weighed to determine dry mass per unit area (g m^{-2}). Herbaceous plant biomass was analyzed for LOI and 1 M HCl-TP using methods described above for soil. TP content for woody biomass was estimated to be 750 mg kg^{-1} based on literature values (Bedford et al., 1999; Cronk & Fennessy, 2001).

3.2.4. Litterfall and Litter Decomposition

Each winter herbaceous plant (macrophyte) biomass senesces and is folded over the soil by snow and ice, so the stock of end-of-season standing herbaceous biomass plus fresh herbaceous plant litter (e.g., dead shoots already fallen) is approximately equal to litterfall production for that year. Aboveground herbaceous biomass and freshly deposited litter was collected in triplicate at each plot from 0.5m^2 quadrats by clipping standing herbaceous biomass to within 1cm of the soil surface then collecting freshly deposited litter within each quadrat in October of 2019 and 2020 (prior to flooding). Litterfall was transported, stored, dried, weighed and homogenized in the same fashion as aboveground biomass. Litter mass decay and net P mineralization was estimated using a litterbag decomposition experiment. Briefly, litterbags were constructed from fiberglass window screen (20 cm × 20 cm; 2-mm mesh) and stainless steel staples. Bags were filled with 10-20g of dry clipped and homogenized litter and labeled with the site, plot, time increment and replicate. In late fall of 2019, five groups of triplicate litterbags were placed at each sampling plot by fastening each to the soil surface with stainless steel 15cm landscaping staples. Litterbags were retrieved in triplicate after incubating for periods of 0, ~100, ~150, ~250, and ~365 days (Chimney & Pietro, 2006). Retrieved litter samples were dried at 60°C for 72hr and weighed to determine mass loss and analyzed for organic content and total P using the LOI and 1 M HCl-TP methods described above.

3.2.5. Accretion

Accretion is the vertical accumulation of material, including macrophyte litter, other detritus, and sediment over the soil surface (Callaway et al., 2013). Accretion rates in the riparian wetlands were measured using ceramic tiles (30.5 x 30.5 cm) (McMillan & Noe, 2017; Callaway et al. 2013), three per plot, placed in early October 2019. Accumulated sediment, detritus, and litter were collected from tiles and bagged during dry conditions in July of 2020. Tiles were replaced and then collected again in July of 2021. Accreted material was stored in pre-weighed and labeled zip-lock bags and then composite samples of accreted material were created. At the lab, live biomass and other contamination (plastic, tile debris) was removed, samples were dried at 60°C and weighed, and then analyzed for LOI, total P, inorganic P, and organic P, following the 3-pool parallel P fractionation method described above for soils (Richardson & Reddy, 2013). The mass of sediment and detritus was then estimated as the difference between total accretion and litter.

3.2.6. Water Monitoring during Flood Events

To monitor surface water stages, we placed water level recorders at high and low elevation plots of each site (OnSET HOBO MX2001-04). The water level recorders were housed inside vented PVC pipes and installed into the ground as shallow groundwater wells. The water level recorders had two pressure transducers separated by 5ft, which allowed for real time local correction for

changes in atmospheric pressure. One pressure transducer was kept aboveground at the high elevation plot of each site and was used to calculate water levels if the water depth above the low elevation recorder exceeded 5ft. At the median elevation plot of each site, we placed optical dissolved oxygen and temperature loggers (PME: miniDOT) equipped with anti-fouling plates and an automated lens wiper (PME: miniWiper).

The water quality monitoring protocol used a combination of autosampling, passive siphon sampling, and grab sampling to capture the dynamics of the first pulse of water entering the wetland with high resolution and long-term dynamics over the course of the flood with coarser resolution. The median elevation plot of each site had one ISCO autosampler (Model 6712, Teledyne Technologies, Inc.) that collected discrete water samples during the first 24hr of inundation. ISCOs were programmed to collect floodwater samples hourly over 24hr after water levels exceeded 10cm above the soil surface. The ISCOs were placed outside the perimeter of the sampling plot and were fastened 1.5m above the sediment surface to a wooden frame. Each ISCO had a 25ft suction-line and strainer that was held at 10 cm above the sediment surface at the center of the sampling plot. An actuator triggered sampling when water levels rose above the strainer (Model 1640, Teledyne Technologies, Inc.).

Each wetland sampling plot also hosted replicate USGS-designed first flush (passive siphon) samplers that collected floodwater samples upon inundation (Diehl, 2007). The siphon samplers consisted of a 1 L narrow mouth amber Nalgene bottle sealed at the top with a no. 7 two-hole rubber stopper. The stopper held a siphon made from copper tubing, and a vent tube made from vinyl tubing that enabled water flow into the bottle after water levels rose above the crest of the copper tubing. The siphons were fixed sideways attached to a pole at each plot center and were positioned to trigger when water exceeded 10cm above the sediment.

To capture longer term water quality dynamics, 1 L grab samples were collected from the river and inflow and outflow channels at each site, as well as at all inundated wetland plots (up to 5 per site) on the rising and falling limbs of flood events. To collect grab samples, wide mouth amber Nalgene bottles were attached to an extendable pole fitted with hose clamps. Field measurements of water temperature, dissolved oxygen (DO, mg L^{-1}), oxidation reduction potential (ORP, mV), specific conductivity (SPC, uS cm^{-1}), and pH were recorded each time a grab sample was taken using a YSI Professional Plus. Each YSI parameter was calibrated daily before each sampling trip and verified with a reference solution. During the three flood pulses that were captured by ISCOs, the sites were monitored daily during the rising limb of floods or until ISCO programs had finished, enabling collection of each sample within the U.S. EPA recommended maximum hold time for SRP of 24hrs (O'Dell, 1993).

All water samples were stored on ice during transport and processed immediately at the University of Vermont Aiken Forestry Sciences Lab. Subsamples of 5 mL volume were filtered (0.45 μm) and frozen until analysis for SRP, while subsamples of 20 mL volume were pipetted into pre-cleaned (acid washed, and 3x rinsed with DDI H_2O) 60 mL borosilicate glass digestion vials and stored in the dark at room temperature for digestion and analysis of total P (TP). The remaining water samples were analyzed for total suspended solids (TSS), as well as mineral (ISS) and organic (OSS) fractions of TSS based on ignition at 550°C (Roy et al., 2016). SRP was analyzed at 660 nm using a microplate reader (BioTek Synergy HT) following the malachite green method for

colorimetric orthophosphate analysis (D'Angelo et al. 2001; Ringuet et al. 2011). TP samples were digested following the alkaline persulfate digestion (Patton & Kryskalla, 2003), and analyzed using colorimetric orthosphosphate analysis at 880 nm on a Lachat QuickChem 8500 using the ascorbic acid method for molybdenum blue (Murphy & Riley, 1962).

3.2.7. Data Analysis

Stocks of P in soil, biomass, litter, and accreted material, were calculated by multiplying the mass stock by P content of the material for a given P pool (Eqn. 6).

$$P_x = C_x * M_x \quad \text{(Eqn. 6)}$$

where, P_x is the stock of phosphorus contained in material X (e.g., g P m^{-2}), C_x is content of P per dry unit material X (e.g., g P g^{-1} dry soil), and M_x is dry mass stock of material X (e.g., g dry soil m^{-2}). For water, P stock was calculated as the product of P concentration (e.g., mg P L^{-1}) and water volume (e.g., L).

Flux rates (e.g., litter decomposition, accretion) were calculated as change in mass or P stock between two time points. Flux rates of P in the water column were quantified as the difference in water column P stocks between time increments, divided by the change in time (Fisher and Reddy, 2001; Roy et al., 2012)

For soil, biomass, litter, and accreted material stocks, we calculated summary statistics (mean, standard deviation), at the plot level by averaging replicates for a given plot, and at the site level by averaging means for all 5 wetland sampling plots. Because the sampling plots were distributed randomly within equal area elevation percentile bins at each site, site level averages from sampling plots represent estimates of spatially weighted averages across the entire sampling zone. We examined correlations amongst different P stocks across all sites using Spearman rank correlation tests. Additionally, we assessed patterns in soil properties, P flows, and P stocks along elevation gradients in each site by performing Spearman rank correlation tests and multiple regression with hydrologic metrics, including fraction of time inundated (ind) and the 90th percentile flooding depth. We compared site-level spatially weighted mean P stocks and fluxes for soil, biomass, litter, and accreted material using the non-parametric Kruskal-Wallace test, followed by a Dunn post-hoc test with Bonferonni adjustment for family-wise error rate (dunn.test package).

For analysis of field water quality data, we classified the water samples based on three categories: the site, the sample origin (inflow/outflow, river, or wetland), and the condition (filling or draining). At Prindle Road, samples were classified as inflow if they were collected at the culverts along Prindle Road and samples were classified as outflow if they were collected from below the beaver dam. At Otter Creek sites (Swamp Road and Union Street), samples were classified as having river origin if they were collected in the river or from ditches when the flow was from the river into the wetland. Samples that were not classified as river, inflow or outflow were defined as having wetland origin. Samples were classified as having the condition of filling if the rate of change in the water level was positive and classified with the condition of draining if the rate of change in the water level was negative. We determined differences in water quality parameters (TSS, ISS, OSS, DO, pH, ORP, SPC, SRP, TP) among the following groupings: (first) origin only, (second) origin and condition, (third) site and origin, and (fourth) site, origin, and condition, using

the Dunn method for the Kruskal-Wallace test with Bonferroni p-value adjustment (dunn.test package). We also fit simple linear regressions to water quality parameters. We used a test-statistic of 0.05 to as the significance threshold in all statistical tests. Throughout the paper we use the following significance codes: *$0.05 > p \geq 0.01$, **$0.01 > p \geq 0.001$, ***$p < 0.001$. All calculations and statistics were performed using R version 4.0.3 (R Core Team).

3.3. Model Calibration & Scenarios

For calibration, verification, and sensitivity analysis, the model was executed using data between 7/15/19 and 7/15/21 for sampling plots 0, 2, and 4 at each site. Year 1 data were used for model calibration. We then examined the simulation results from year two data to verify the model performance; and both years of data were used to evaluate various scenarios for a sensitivity analysis.

Data preprocessing was required prior to model execution. The dry mass and P stocks of biomass (aboveground shoots and belowground roots), and soil were set to the mean values from samples collected in summer of 2019. The parameters for adsorption, assimilation (uptake of P into plant biomass), and decomposition, were set to our best guess by adjusting their values within their range reported in the literature until biomass, inorganic P deposition, and litter were all clustered near the 1:1 line on plots of modeled versus measured results. The inflow concentrations of various P stocks were estimated from median values of TSS, including total suspended solids (mg d.w./L), total P (mg TP/L), the organic fraction of TSS (mg d.w./mg d.w.), and the soluble-reactive fraction of TP (mg P/mg P). Equilibrium DIP (DIP_E) was set to the final SRP concentration from the aerobic laboratory intact core incubations corresponding with each plot. The aerobic intact core incubation results were used because our high frequency *in situ* data suggests that diurnal fluctuations in dissolved oxygen occur at the sediment-water interface in the field (most likely due to the dynamics of photosynthesis and respiration). This phenomenon was most similar to our lab aerobic incubation experiments where water columns above intact cores were reaerated using room air 1x per day.

Preprocessed model inputs also included water elevation and temperature recorded by HOBO MX2001 at 10-minute intervals, and sub-hourly meteorological data from the Burlington airport (NOAA NCDC) used to estimate precipitation and evapotranspiration. The HOBO data were summarized to daily values by taking the average temperature, and the maximum water height each for each calendar date in the record, then converted to estimates of water height and storage volume (m^3/m^2) for each plot. The meteorological data were summarized to daily values by averaging temperature, wind speed, and relative humidity, and by summing precipitation. Evapotranspiration rates were estimated with the meteorological data using the Penman-Monteith method using cloud cover, temperature, relative humidity, and windspeed (r `evapotranspiration` package). Net surface flow was estimated by adjusting changes in water volume for estimated precipitation and evapotranspiration. Inflow and outflow were deduced from net surface flow by adding a term for throughflow, which was calculated as the water volume divided by hydraulic residence time (Appendix A). Hydraulic residence time was modeled according to a negative power law relationship with elevation relative to the lowest elevation sampling plot that was calibrated to each site (Appendix A).

Model input parameters fall into three groups: (A) local (measured) parameters, (B) stochastic (unmeasured) parameters, and (C) universal parameters. Universal parameters are precisely known, and do not vary within the model scope (e.g., the viscosity of freshwater water at 20^0C, the particle density of inorganic sediments). The values for universal parameters were taken directly from literature values. The distinction between local and stochastic parameters is the feasibility of their measurement/derivation. Local parameters vary from site to site and are feasibly measured or derived across many sites. These include parameters that define the initial conditions of state variables (soil, water, vegetation), hydrologic flows, and inflow concentrations. The values for local parameters were taken from field/lab measurements from this study. Stochastic parameters may or may not vary from site to site but are impractical to measure at a wide number potential wetland restoration sites (many thousands have been identified in Vermont). Stochastic parameters in the model tend to be rate coefficients that affect process flows (e.g., the rate of decay of plant litter) or partitioning coefficients that relate the size of one pool to the size of another (e.g., the labile fraction of decomposing litter).

Following calibration and verification of the model, a sensitivity analysis was performed involving various scenarios designed to elucidate hydrologic versus biogeochemical controls on net P retention within riparian wetland ecosystems. Scenarios included changes in inflow P concentrations, changes in hydraulic residence time, and changes in water levels at median elevation plots for each site. Identification of feasible ranges in hydrologic variables at the two Otter Creek sites (Union Street and Swamp Road) were informed by review of existing models for the region, including a 2D HEC-RAS model for the Otter Creek (Trueheart, 2019). At the Prindle Road site, we developed a rainfall/runoff model using HydroCAD (HydroCAD Software Solutions, LLC) which simulated the wetland as a pond with stage-volume relationships defined by minimum 1-meter resolution Digital Elevation Model and a beaver dam for a downstream outlet (Augustin, 2021). However, we decided to discontinue HydroCAD model development for two primary reasons: (1) Field data indicated that the beaver dam outlet of the Prindle Road site was dynamic during our study period, leading to a changing relationship between water level and outflow that made calibration/verification of the model impossible. (2) We were instead able to use field measurements (including at the system outlet) to estimate the relationship between hydraulic retention time and water level throughout the study, fulfilling the goal of the initial HydroCAD effort in a more straightforward manner.

We ran all scenarios over the two-year monitoring period with our calibrated model using either siphon data collected at sampling plots or stream (i.e., river) concentrations. The simulations using siphon data included the default parameters and used data from median estimates from passive siphons as inflow TSS and P concentrations to sampling plots. The siphon simulations are useful for calibration and verification but do not necessarily provide a representative estimate of how the whole system is functioning. For example, sediments are deposited and dissolved P may flux out of soils as stream water passes through the wetland on its way to each sampling plot. Simulations using median concentrations from the samples collected at stream inflow locations therefore provide a more representative estimate of the ecosystem level P retention. We tested model sensitivity to increasing and decreasing HRT across various simulations including different assumptions for inflow TSS and P concentrations. We also tested a 20% increase in water levels at median elevation plots for each site compared to our field observations using predictions of HRT based on water level.

Scenarios altering HRT or water levels provide insights into how system hydrology affects net P retention. Such changes could potentially occur as a result of restoration actions that alter site hydrology, changes in land management that affect peak flows, year to year variability in precipitation patterns, or climate change. Scenario testing used to investigate biogeochemical control on wetland P retention included running model simulations using different inflow sediment and phosphorus concentrations. Such differences could in reality be driven by upstream land management (e.g., P load reductions resulting from agricultural best management practices) or wetland landscape position.

To contextualize our model scenarios, we examined flow duration curves for USGS streamflow gaging records on the Otter Creek and Lewis Creek to better understand historic trends in the frequency and magnitude of overbank flooding events, which characterize the hydroperiod of our studied wetlands. We were able to investigate potential historic shifts in the Otter Creek flow duration curve due to the 90+ year record available. However, only ~30 years of data were available for Lewis Creek, which limited our ability to identify potential historic shifts.

4. Quality Assurance Tasks Completed

All data presented in this report were reviewed by the UVM Project QA Officer (Adrian Wiegman) and the UVM Project Manager (Dr. Eric Roy) for logical consistency and coding errors. Dr. Eric Roy was responsible for oversight of sample handling, laboratory procedures, data analysis, modeling, and data visualization. Quality assurance protocols, as described in the project QAPP, were followed, a portion of which are described below.

- For each lab procedure, one in every ten discrete field samples was randomly selected to be analyzed in duplicate. At least one replicate sample was analyzed in each batch. All laboratory samples analyzed with colorimetric chemical tests in microplates were conducted in triplicate to ensure that results are representative. Duplicate, blank, and QC standard samples were analyzed for every microplate and ~10% of microplates also included laboratory spikes. Performance was analyzed for any given analyses using criteria defined in the project QAPP. If replicate samples failed to meet performance standard described below, the sample set was re-analyzed. For data used in this report, QC standards fell within acceptable limits (within ±10% of known values), laboratory blanks indicated no contamination present and duplicates were within ±10% of each other. All laboratory spikes analyzed were also within ±10% of target values.
- All soil, biomass and litter samples were collected in replicate at the plot level. Passive siphon water samples were collected in duplicate at the plot level. Every 10th water grab sample was collected in duplicate. ISCO water samples suction lines were fitted with a strainer tube that enabled water to be collected from multiple points. Passive siphon samples and ISCO samples were compared against each other. Steps were taken to preserve the integrity of samples using the criteria described in the project QAPP.
- All biomass and litter samples were clipped to 10cm then ground on a Wiley mill to 1mm. Dried soil, biomass, and litter samples were stored at room temperature (20-25°C) in plastic containers. All filtered extracts for chemical analysis (water, soil, biomass, etc.) were either immediately frozen or processed within 72 hours from time of sample collection and always maintained at temperatures 4°C (±1°C). Samples stored at the incorrect temperature were not analyzed.

- Prior to use, all samplers and tools were vigorously cleaned with a phosphorus free detergent (i.e., Alconox) and rinsed generously with distilled water. Between deployments and between sites, the samplers and sample bottles were cleaned and rinsed three times with distilled water. Lab plastic sample containers (if not new) and glassware were acid washed (1 M HCl for 2+ hours) and triple rinsed with DI water prior to use.
- Invasive species spread was controlled by rinsing boots/waders/equipment with Sparquat 256 (or a similar cleaner).
- All supplies and consumables for field and laboratory activities were inspected for compliance with the acceptance criteria by qualified laboratory staff prior to use.
- Laboratory and field instrumentation and equipment use followed manufacturer instructions and accepted procedures associated with the selected analytical methods.
- Consistent sample labeling schemes were employed throughout the study.
- All data collected in the field were georeferenced to sub-meter horizontal accuracy using an Emlid Reach RS+. Latitude, longitude and altitude (measured as height above ellipsoid in meters) were recorded by the Reach RS+ in the WGS 1984 datum. The Reach RS+ was mounted on a pole that rests on the ground surface at a known and recorded height above the ground surface. Measurements were postprocessed to improve accuracy based on simultaneous measurements at a reference station according to Emlid differential GPS protocols.
- A DEM generated from LiDAR data and field surveys was used to estimate water storage volumes. LiDAR elevation data do not penetrate below water surfaces and available flights may be over 5 years old, which means restoration features could be missing. To minimize site disturbance, only crucial features and plot marker poles were surveyed. During a dry period in the first summer, the edges and mid points of crucial features such as river beds, ditches, ridges, ditch plugs and ponding were georeferenced and their dimensions were recorded. A LiDAR elevation dataset was adjusted based on the average difference between the elevation at sample plot marker poles and the elevation of the overlapping LiDAR pixels.
- The Wetland P Model was developed using best practices for data storage and version control and will be stored on a password protected repository hosted by the private UVM Gitlab repository (https://gitlab.uvm.edu/). It is currently stored on a private password protected repository on Mr. Wiegman's GitHub page (https://github.com/arhwiegman/wetlandP).
- Three project team members with advanced training reviewed the modeling inputs and results described in this report.
- Any reference in this document to data or values obtained from "literature" refers to either: (1) peer reviewed scholarly journal articles or edited book chapters available within the online databases of Elsevier, Springer, Wiley, Web of Science, or other databases available within the University of Vermont Bailey Howe Library online catalog, or (2) local information provided by reputable government, private industry, and non-profit sources, including white papers, data reports, and data generated by the project team in other projects following the methods detailed in our project QAPP.
- All electronic files were backed up on a regular basis. At the conclusion of the project all relevant information, project files and electronic data will be turned over to the LCBP Project Manager for archiving. The files will be archived for a minimum of 5 years following completion of the project.

5. Deliverables Completed

5.1. Initial Model Development

Initial development of the Wetland P Model was completed as described in the project QAPP and included defining numerous state variables, flows, and rates (Figure 4 and Table 2). Our primary objective during development was for the model to be able to simulate the key processes influencing net P retention in a riparian wetland during flood inundation events, including P deposition and dissolved P dynamics. Modeling these processes required representation of P transport into and out of the wetland system with floodwater, inorganic P chemistry (sorption/desorption), particle settling, diffusion at the sediment-water interface, and transformations of organic P to inorganic P (mineralization) (Reddy and Delaune 2008). This was accomplished by including aboveground and belowground compartments with biomass, organic, and inorganic P stocks, linked by various flows that could be calibrated based on our field measurements or literature values (Figure 4). We provide a detailed description of the model in Appendix A.

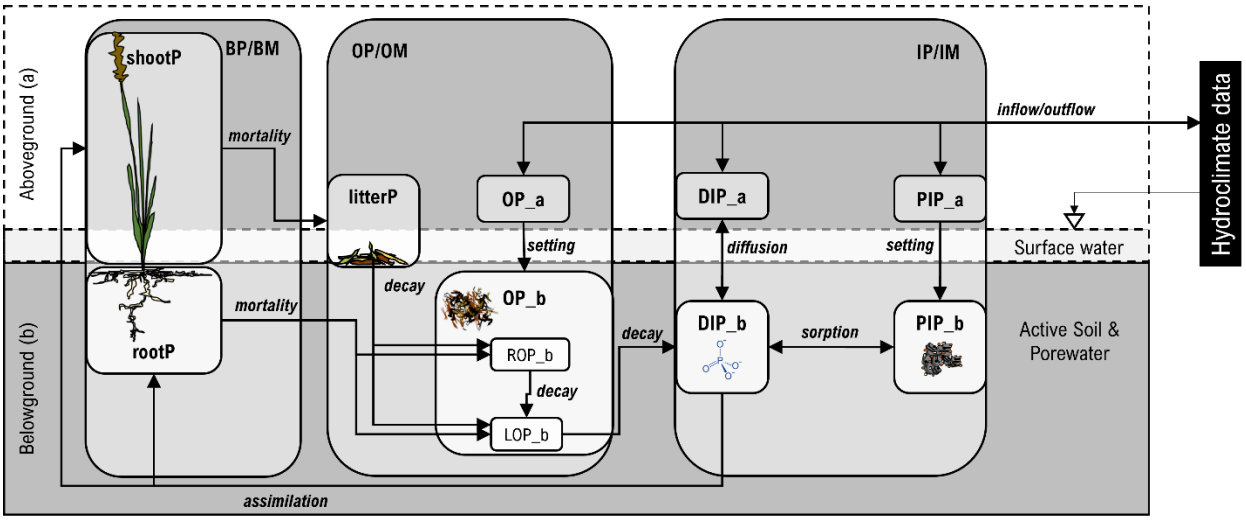

Figure 4. Conceptual diagram of model domain, compartments, state variables, and processes. Flows of phosphorus are represented by lines with arrows and the associated process for each flow is labeled in italics. State variables are represented in boxes with rounded edges.

Table 2. State variables calculated with ordinary differential equations in the model.

Name	Unit	Description
IM_a	g d.w	inorganic matter aboveground
IM_b	g d.w	inorganic matter belowground
shootP	g P	aboveground live shoot P
rootP	g P	belowground live root P
litterP	g P	aboveground litter P
ROP_a	g P	refractory OP aboveground
LOP_a	g P	labile OP aboveground
PIP_a	g P	particulate IP aboveground
DIP_a	g P	dissolved IP aboveground
ROP_b	g P	refractory OP belowground
LOP_b	g P	labile OP belowground
PIP_b	g P	particulate IP belowground
DIP_b	g P	dissolved IP belowground

Key model assumptions include the following:

1. DIP (i.e., SRP) adsorption
    a. Oxalate extractable Al plus Fe represents the maximum storage (i.e., sorption) capacity for exchangeable P in the soil (PSC, mg P/kg) [PSC = 31/(Al/27+Fe/56)]. Here, PSC is referred to as Ex_max, the variable name used in the Wetland P Model. Oxalate extractable P represents the exchangeable inorganic P pool (Ex). Therefore, the product of the Oxalate P Saturation Ratio (PSR, mol/mol) [PSR = (P/31)/(Al/27 + Fe/56)] and Ex_max was used to initialize the particulate inorganic P (PIP) pool in the model's belowground compartment.
    b. Based on our field observations, riparian/floodplain wetland water columns experience intermittent periods of aerobic and anaerobic conditions. We therefore decided to use equilibrium DIP values in our modeling that were based on the final SRP concentrations observed during the aerobic (O_2) treatments in the laboratory intact core experiments. Those experimental treatments included daily reaeration with subsequent declines in DO, similar to most of our field observations. Langmuir model parameters have been used in past models to simulate equilibrium P dynamics (e.g. Wang et al., 2003). However, we found poor correlation between Langmuir model parameters and SRP fluxes in our laboratory intact core experiments.
2. Inorganic soil accretion (settling, outflows)
    a. There is no significant bioturbation effect.
    b. Adsorption occurs only below the soil surface and does not occur in the water column.
    c. Inflow concentrations of inorganic sediments, as well as dissolved and particulate inorganic P, are derived from median stream concentrations of TSS and TP unless otherwise noted.
3. Organic soil accretion (growth/decay, inflows)
    a. There is one generalized type of primary producer that synthesizes aboveground and belowground biomass in equal proportion, but with differing turnover rates. Aboveground biomass turns over at least once per year with winter senescence, while belowground biomass can take many years to turnover.
    b. Tissue concentrations of P are the same across all forms organic matter, live biomass, or litter, including labile and refractory organic matter.
    c. The decomposition rate coefficient of labile organic matter is affected only by temperature. Refractory organic matter, which represents lignin-rich material (phenolic compounds; Morris et al., 2016), does not decompose when the wetland is inundated (Freeman et al., 2001). However, when water falls below the wetland surface, refractory organic matter decomposes in the same fashion as labile organic matter, but with a much lower rate coefficient.
    d. Inflow concentrations of labile and refractory organic sediments and P are derived from median stream/inflow concentrations of TSS and TP.

Preliminary testing of the model included inspection of time series plots for model state variables, visual comparison of state variable values with field observations, confirmation of model mass

balance, and evaluation of model performance under increasing complexity of simulation (see Appendix A for full description of testing). Based on these evaluations, we deemed model performance acceptable and proceeded to the calibration phase following the collection of field data.

5.2. Field Studies

5.2.1. Soil Analyses

Table 3 shows spatially weighted averages at the site level for soil properties in the 0-5cm and 5-10cm soil layers. The levels of soil moisture (MC), bulk density (BD) and organic matter (LOI) were not significantly different across sites for both soil layers. Site-wide averages in the 0-5cm layer ranged from 57% to 67% for MC, 0.32 to 0.38 g cm^{-3} for BD, and 22% to 30% for LOI. The soil layers differed in some cases in terms of MC, BD, and LOI, with lesser MC, greater BD, and lesser LOI in the 5-10 cm layer compared to the 0-5 cm layer (differences especially pronounced for Prindle Road).

Table 3. Spatially weighted averages (±1 standard deviation) for soil properties at each site by depth. Letters in common across rows (site and depth) indicate no significant difference in median value (Dunn-Bonferroni).

site	Prindle Road		Union Street		Swamp Road	
Soil depth	**0-5cm**	**5-10cm**	**0-5cm**	**5-10cm**	**0-5cm**	**5-10cm**
MC (%)	a 67 ± 11	b 44 ± 11	ab 57 ± 12	b 47 ± 9	ab 60 ± 19	b 44 ± 11
BD (g/cm^3)	a 0.32 ± 0.15	b 0.73 ± 0.22	ac 0.38 ± 0.10	bc 0.58 ± 0.11	ac 0.36 ± 0.18	b 0.64 ± 0.15
LOI (%)	a 27 ± 6	b 16 ± 4	ab 22 ± 9	ab 20 ± 9	ab 30 ± 20	b 17 ± 8
Al-3051a (g/kg)	a 27.8 ± 3.6	ab 30.8 ± 5.2	bc 20.2 ± 1.4	c 20.1 ± 1.4	bc 22.7 ± 3.0	bc 25.2 ± 5.0
Ca-3051a (g/kg)	a 8.07 ± 1.1	ab 6.23 ± 1.1	b 4.51 ± 0.7	b 3.65 ± 0.4	a 4.73 ± 1.1	ab 4.44 ± 0.9
Fe-3051a (g/kg)	ab 20.2 ± 3.6	a 23.8 ± 4.8	abc 28.4 ± 2.6	bc 28.1 ± 3.1	c 22.4 ± 2.9	bc 23.7 ± 2.1
Mg-3051a (g/kg)	a 6.95 ± 1.0	a 7.61 ± 1.2	a 6.01 ± 0.6	a 5.75 ± 0.5	a 5.63 ± 0.01	a 5.86 ± 0.8
HCl-Pi (mg/kg)	a 333 ± 60	b 313 ± 85	a 388 ± 120	ab 332 ± 93	a 396 ± 44	ab 357 ± 39
HCl-TP (mg/kg)	a 1140 ± 160	b 788 ± 180	a 1140 ± 150	ab 1060 ± 140	a 1260 ± 230	ab 1050 ± 180
Ox-Al (mg/kg)	a 2090 ± 480	a 2500 ± 680	a 1960 ± 220	a 1910 ± 230	a 1910 ± 480	a 1920 ± 610
Ox-Fe (mg/kg)	a 2550 ± 460	a 2640 ± 660	b 6110 ± 1500	b 5790 ± 1200	a 3090 ± 710	a 3080 ± 1600
Ox-P (mg/kg)	ab 407 ± 57	a 342 ± 86	c 644 ± 120	bc 577 ± 75	c 662 ± 150	c 625 ± 130

Soil aluminum (Al) and iron (Fe) can play important roles in wetland P cycling. There were significant differences in the levels of total and oxalate extractable Al and Fe between sites, notably Al-3051a, Fe-3051a, and Fe-ox (Table 3). Union Street had significantly lower levels of total Al (Al-3051a = ~20 g Al kg^{-1}), compared to Prindle Road (Al-3051a = ~29 g Al kg^{-1}). At Swamp Road, Al-3051a was slightly higher than Union Street and lower than Prindle Road, but not significantly different from either site. Oxalate extractable Al (Al-ox) ranged from 1.91 in the 5-

10cm layer at Union Street, to 2.50 in the 5-10cm layer at Prindle Road but did not differ significantly across sites or depths. At Union Street, both total and oxalate extractable Fe were greater than at Swamp Road and Prindle Road (Table 3).

The sites did not differ significantly in terms of mean inorganic P (HCl-Pi), organic P (HCl-Po), or total P (HCl-TP, mg P kg^{-1}). HCl-Pi ranged from 313 to 396 and did not differ by site or depth. HCl-Po (which ranged from 476 to 861) and HCl-TP (which ranged from 788 to 1260) differed in some cases by depth within sites but did not differ significantly between sites for either depth layer. The two Otter Creek sites both had similar levels of oxalate extractable P (P-ox) near ~600 mg P kg^{-1}, which were greater than at Prindle Road (~400 mg P kg^{-1}, Table 3).

Figure 5 shows mean results of the sequential P fractionation scheme by site, depth, and sampling plot. The majority of soil P in both 0-5 cm and 5-10 cm layers was contained within organic fractions, with the relative size of NaOH-Po versus residual P varying across sites (Figure 5). The relative proportion in residual P pool was greater at Lewis Creek compared to the two Otter Creek sites. For most plots, the 0.5 M HCl-Pi pool from the sequential fractionation, which has been operationally defined to contain primarily Ca- and Mg-bound P, was the largest inorganic P pool. However, the NaOH-Pi pool, which contains Al- and Fe-associated P was also prominent at the two Otter Creek sites, especially at lower elevation plots. The sum of P fractions with the most potential to eventually become bioavailable (Exchangeable P + NaOH-Pi + NaOH-Po) as a percentage of frac-TP, equaled 29±18% and 30±21% at Prindle Road, 50±8.1% and 52±11% at Union Street, and 54±7.6 % and 53±4.6% at Swamp Road, in the 0-5cm and 5-10cm layers, respectively.

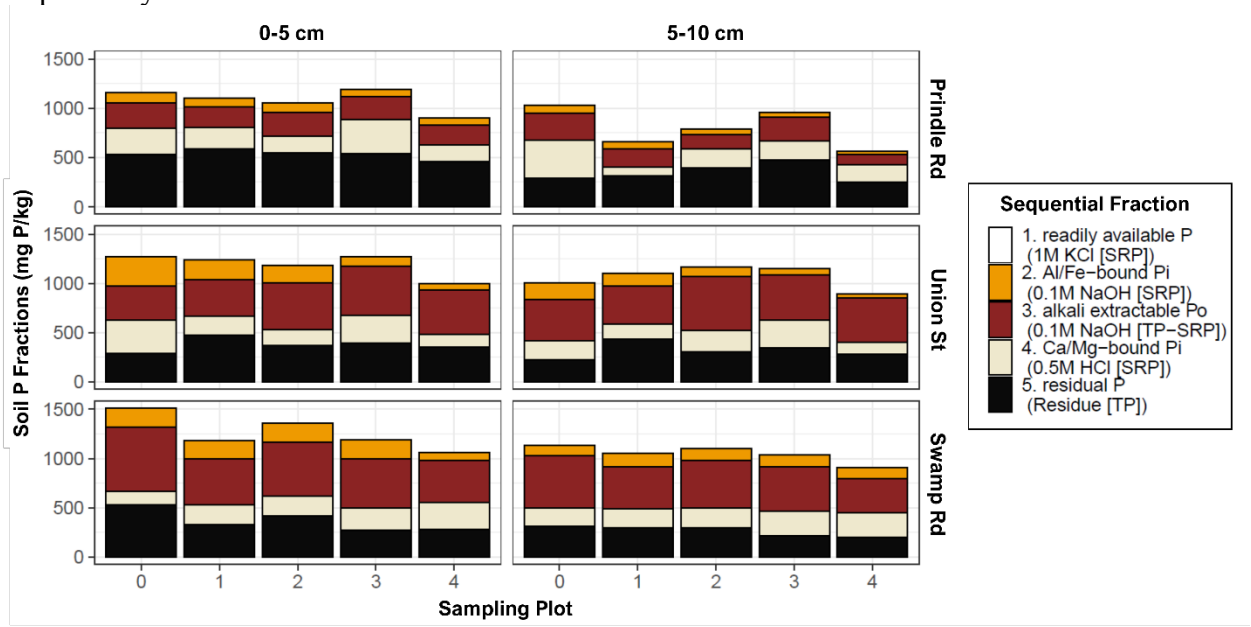

Figure 5. Soil P fractions of soil at each sampling plot faceted by depth (columns) and site (rows). Inorganic P (P_i) includes fractions 1, 2, and 4 in the legend. Organic P (P_o) includes fractions 3 and 5 in the legend.

Plot-level mean total P estimated by the sum of all sequential P fractions (frac-TP, mg P kg^{-1}) ranged from ~900 (Prindle Road, plot 4) to ~1500 (Swamp Road, Plot 0) and ~560 (Prindle Road, plot 4) to 1160 (Union Street, plot 2) for the 0-5 cm and 5-10 cm layers, respectively. There was some evidence of increasing total P with decreasing elevation (adj-$r^2 = 0.43$, $p = 4.2E\text{-}7$). The three

methods used to measure soil total P (frac-TP, 1 M HCl-TP, and 3051a-TP) were in good agreement (Figure 6). The sum of organic pools in the sequential fractionation (frac-P_o) were well correlated with organic P estimated using the 3 pool parallel fractionation (1M HCl-P_o) (r^2 = 0.67, p = 4E-17). Similarly, the total inorganic P estimated by the sequential (frac-P_i) and parallel (1 M HCl-P_i) schemes were generally well aligned (r^2 = 0.52, p = 7.9E-11), however, the regression fit deviated significantly from a 1:1 line even after removing outlier and leverage points (Figure 6). This suggests that the 1 M HCl-Pi method might overestimate inorganic P in some cases, especially when present in relatively lower amounts. The three-pool parallel fractionation for total, inorganic, and organic P using 1 M HCl is far easier to perform and inexpensive compared to the sequential P fractionation method. Results in Figure 6 indicate that the three-pool parallel P fractionation protocol we used in this project provides acceptable results for P forms of interest in riparian wetlands in the Lake Champlain Basin.

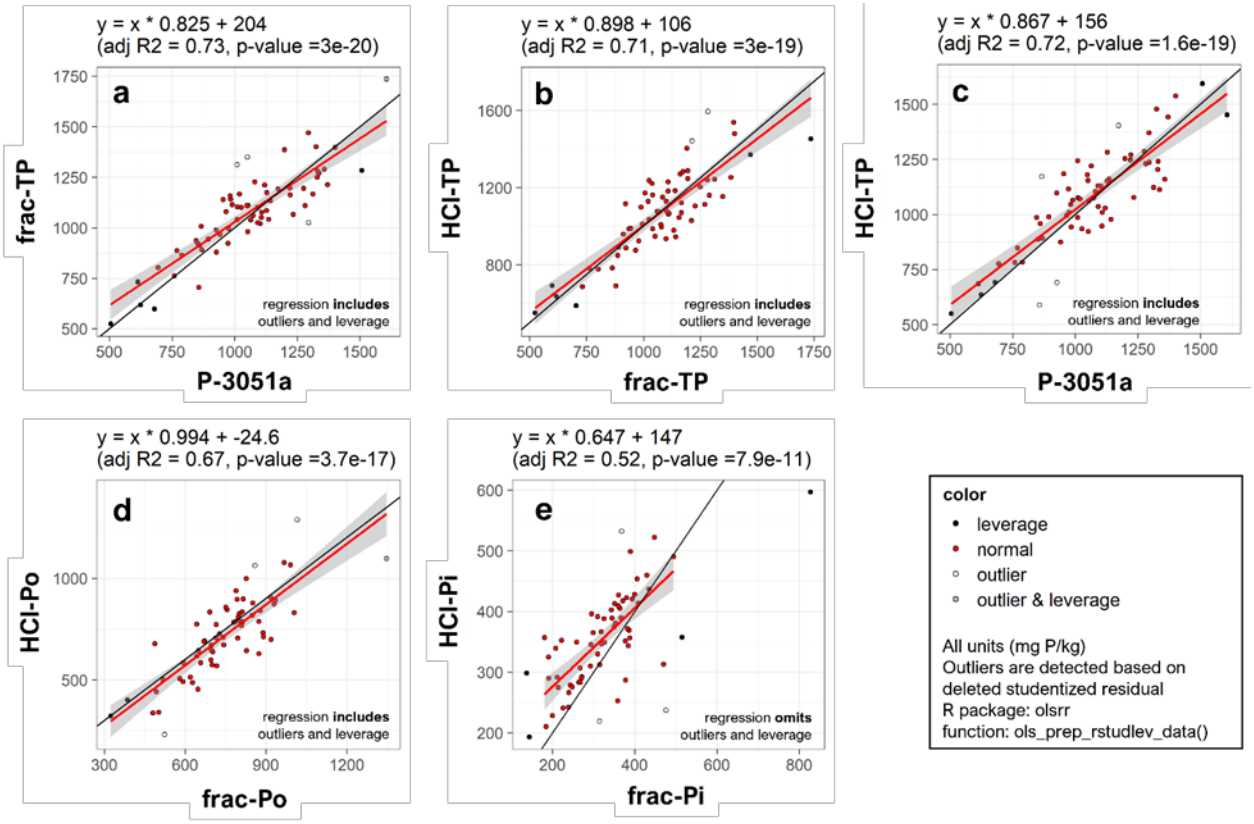

Figure 6. Comparison of soil P fractions estimated from different methods. The top row compares total P methods: P-3051a vs frac-TP (a), frac-TP vs HCl-TP (b), and P-3051a vs HCl-TP (c). The bottom row compares organic (d) and inorganic (e) P measures from the sequential and parallel schemes used. All regressions include leverage and outlier points except for inorganic P (e). The red line is the regression fit and the black line is the 1:1 line.

The spatially weighted mean of stocks of P in the top 0-10 cm of soils were on the order of ~50 g P m^{-2} at each site (see section 5.2.3 for tabular results). Stocks of soil TP (g P m^{-2}) were 44.4 ± 10.5 at Prindle Road, 52.3 ± 10.9 at Union Street, and 53.7 ± 13.6 at Swamp Road. At each site, organic P made up the majority of the TP stock. The difference in TP stocks between Prindle Road and the Otter Creek sites was explained by Prindle Road having 20% lower stocks of HCl-P_o than the Otter Creek sites. Of the Otter Creek sites, Swamp Road and Union Street had similar stocks

of TP but were differentiated by Swamp Road having slightly higher stocks of HCl-P_i despite having similar or lower stocks of HCl-P_o.

5.2.2. Diffusion of SRP from Soils during Inundation

Table 4 shows mean soil to water SRP flux rates measured over the first 7 days after simulated flooding inside intact cores and common soil metrics used to estimate SRP release risk for the top 0-5cm soil layer. SRP flux rates (g P m^{-2} d^{-1}) ranged from 0.002 for the aerobic treatment at the plot 2 of Union Street to 0.031 for the anaerobic treatment at plot 2 of Swamp Road. In all cases the anaerobic treatment (cores purged 90 min/d with 100% N_2) yielded higher flux rates that the aerobic treatment (cores purged 90 min/d with 20% O_2). For the anaerobic treatment, Swamp Road had the highest SRP flux rates (g P m^{-2} d^{-1}) at approximately 0.023, followed by Prindle Road at approximately 0.02, then Union Street at approximately 0.006. For the aerobic treatment, Prindle Road had the highest flux rates (g P m^{-2} d^{-1}) at approximately 0.009, followed by Swamp Road at approximately 0.006, then Union Street at approximately 0.003.

Table 4. Soil to water SRP flux rates observed in simulated floods inside intact cores (average flux rate over the first 7 days after flooding) and related soil properties (reported as averages for the top 0-5cm).

site	**Prindle Road**			**Union Street**			**Swamp Road**		
plot	**0**	**2**	**4**	**0**	**2**	**4**	**0**	**2**	**4**
Intact Core SRP flux rates (g P m^{-2} d^{-1}) - Day 0 to 7									
Anaerobic	0.024 ± 0.017	0.019 ± 0.008	0.017 ± 0.003	0.009 ± 0.005	0.004 ± 0.001	0.005 ± 0.002	0.029 ± 0.015	0.031 ± 0.024	0.01 ± 0.005
Aerobic	0.004 ± 0.002	0.008 ± 0.006	0.015 ± 0.016	0.003 ± 0.001	0.002 ± 0.001	0.003 ± 0.001	0.006 ± 0.003	0.007 ± 0.004	0.004 ± 0.001
Soil Properties - Depth 0 to 5cm									
WEP (mg/kg)	0.47 ± 0.25	0.13 ± 0.13	0.18 ± 0.27	0.57 ± 0.29	0.07 ± 0.11	0.06 ± 0.09	2.45 ± 2.35	0.27 ± 0.41	0.44 ± 0.22
Ox-[P:Fe] (mol/mol)	0.35 ± 0.02	0.3 ± 0.04	0.27 ± 0.01	0.25 ± 0.05	0.22 ± 0.03	0.16 ± 0.03	0.37 ± 0.1	0.53 ± 0.1	0.23 ± 0.01
Ox-[P:Al] (mol/mol)	0.18 ± 0.2	0.17 ± 0.25	0.15 ± 0.14	0.26 ± 1.28	0.29 ± 0.25	0.23 ± 0.95	0.24 ± 0.22	0.31 ± 0.25	0.37 ± 0.22
Ox- PSR (mol/mol)	0.12 ± 0	0.11 ± 0.01	0.1 ± 0	0.13 ± 0.02	0.12 ± 0.01	0.09 ± 0.02	0.14 ± 0.02	0.2 ± 0.01	0.14 ± 0.01
Ox-SPSC (mg/kg)	339 ± 35	457 ± 40	484 ± 82	539 ± 155	543 ± 113	672 ± 97	324 ± 61	127 ± 60	311 ± 55
S_{max} (mg/kg)	635 ± 23	558 ± 25	438 ± 8	652 ± 7	653 ± 5	586 ± 30	925 ± 9	644 ± 23	405 ± 21
K_L (L/mg)	0.035 ± 0.003	0.063 ± 0.009	0.082 ± 0.005	0.328 ± 0.015	0.282 ± 0.009	0.056 ± 0.009	0.054 ± 0.001	0.144 ± 0.02	0.101 ± 0.019
EPC_0 (mg/L)	2.47	0.46	0.2	0.05	0.06	0.27	1.16	0.23	0.09

Soil metrics that are potentially related to SRP flux from soils are shown in Table 4 (0-5 cm soil layer). Correlation with anaerobic SRP flux rates was strongest for the molar ratio of oxalate

extractable P to Fe (r = 0.97, p = 0.00017), followed by Ox-SPSC (r = -0.82, p = 0.011) and Ox-Fe (r = -0.72, p = 0.037). Correlations were not significant between anaerobic flux rates and WEP, Ox-[P:Al], Ox-PSR, S_{max}, K_L, or EPC_0. Aerobic SRP flux rates were significantly correlated only with Ox-Fe (r = -0.72, p = 0.037).

We show results from SRP flux studies using intact cores for 20 total riparian plots in the Lake Champlain Basin, including the 9 plots included in this LCBP-funded project (3 plots per site) and 11 additional plots from 11 other sites with various land use histories studied as part of separate research in Figure 7. In all cases, sites were either active farm fields or former farm fields that had been restored to wetlands (with varying years since farming). Figure 7 shows final SRP concentrations after 10-14 days of incubation, which can be interpreted as an alternative estimate of equilibrium SRP concentrations to the EPC_0 determined using sorption isotherms (Graetz & Nair, 2009). Within the overall data set, Union Street plots exhibited the lowest SRP release, while Prindle Road and Swamp Road plots fell in the middle range of SRP release during intact core experiments. Across all 20 plots, including the 9 LCBP project plots, statistical analysis indicates that the molar ratio of Ox-P to Ox-Fe, Ox-SPSC, agricultural land use, and Ox-PSR are all strong predictors ($r^2 \geq 0.50$, $p < 0.001$) of SRP diffusive flux in intact core incubations based on simple linear regression. This suggests that soils and past land use moderate release of legacy P from soils during inundation events.

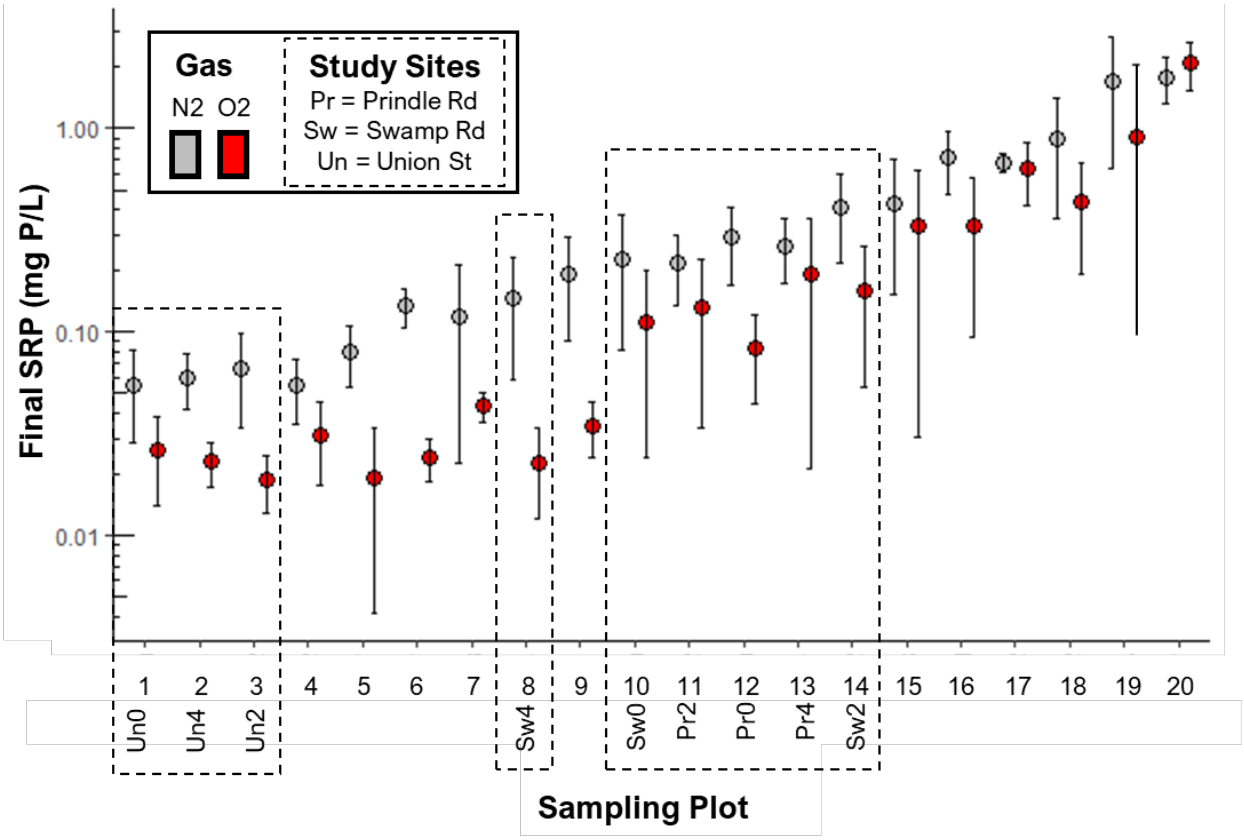

Figure 7. Final SRP (mg P L^{-1}, mean ± 1 standard deviation for days 10 – 14) during intact soil core incubations based on 3 cores per treatment for each sampling plot. Color denotes water column gas treatment: aerobic (room air with O_2, red) and anaerobic (N_2, grey). Plots from this LCBP project are labeled in the figure. Pr = Prindle Road, Un = Union Street, Sw = Swamp Road, 0 = low elevation plot, 2 = median elevation plot, 4 = high elevation plot.

5.2.3. Vegetation Biomass

Spatially weighted averages at the site level for above and belowground biomass and litterfall production are given in Table 5 and are summarized below.

Table 5. Total mass and P stocks by site (mean ± standard deviation, units given in table). Significant differences across sites are denoted by superscript lowercase letters, differences are determined based on the Kruskal-Wallace test with Dunn-Bonferonni post-hoc adjustment. Abbreviations: TM = total mass, IM = mass of inorganic material, OM = mass of organic material, C = P content of material, dw = dry weight.

Site	Prindle Road	Union Street	Swamp Road
Above Ground Woody Biomass (live, diameter measurements, 8/13/21)			
TM (g dw m^{-2})	0	362	17456
TP (g P m^{-2})	0	0.27 ± 0.09	13.1 ± 4.4
Above Ground Herbaceous Biomass (live, clipped to 1cm of soil, 9/2/19)			
TM (g dw m^{-2})	386 ± 292^{ab}	704 ± 352^{a}	374 ± 262^{b}
C (mg P/kg)	1135 ± 335	1854 ± 415	2892 ± 877
TP (g P m^{-2})	0.385 ± 0.286	1.25 ± 0.543	0.891 ± 0.519
Below Ground Biomass (Roots, 0-10cm, wet sieved to >1mm, 9/2/19)			
TM (g dw m^{-2})	1135 ± 397^{ab}	1390 ± 737^{a}	812 ± 409^{b}
C (mg P/kg)	1164 ± 179	1536 ± 297	1269 ± 176
TP (g P m^{-2})	1.314 ± 0.454	2.202 ± 1.583	1.033 ± 0.513
Aboveground Litter Production (Live herbaceous & fresh surface litter, 10/14/19)			
TM (g dw m^{-2})	402 ± 169	472 ± 103	406 ± 180
C (mg P/kg)	1524 ± 705	979 ± 269	1477 ± 222
TP (g P m^{-2})	0.6 ± 0.4	0.47 ± 0.18	0.61 ± 0.32
Aboveground Litter Production (Live herbaceous & fresh surface litter, 10/15/20)			
TM (g dw m^{-2})	419 ± 220^{a}	795 ± 324^{b}	559 ± 212^{ab}
C (mg P/kg)	1524 ± 705	979 ± 269	1477 ± 222
TP (g P m^{-2})	0.61 ± 0.56	0.78 ± 0.37	0.83 ± 0.36
Surface Accretion (30cm^2 tiles, incubated 10/1/19 to 7/15/20)			
TM (g dw m^{-2} yr^{-1})	412 ± 102	469 ± 117	463 ± 106
IM (g dw m^{-2} yr^{-1})	43 ± 17	81 ± 68	94 ± 44
OM (g dw m^{-2} yr^{-1})	369 ± 92	388 ± 99	369 ± 82
TP (g P m^{-2} yr^{-1})	0.62 ± 0.36	0.71 ± 0.36	1.11 ± 0.53
IP (g P m^{-2} yr^{-1})	0.17 ± 0.09	0.37 ± 0.24	0.6 ± 0.34
OP (g P m^{-2} yr^{-1})	0.45 ± 0.28	0.34 ± 0.14	0.51 ± 0.2
Soil (0-10cm, sieved to <2mm, ground, 7/15/20)			
TM (g dw m^{-2} yr^{-1})	52100 ± 16900	48300 ± 9800	49500 ± 15400
IM (g dw m^{-2} yr^{-1})	42300 ± 15200	38700 ± 10500	40200 ± 14600
OM (g dw m^{-2} yr^{-1})	9800 ± 2100	9600 ± 3000	9300 ± 3700
TP (g P m^{-2} yr^{-1})	44.4 ± 10.5	52.3 ± 10.9	53.7 ± 13.6
IP (g P m^{-2} yr^{-1})	15.8 ± 3.3	16.3 ± 2.7	18.6 ± 6.7
OP (g P m^{-2} yr^{-1})	28.6 ± 8.5	36 ± 9.8	35 ± 8.4

Aboveground woody biomass was not present at any of the Prindle Road plots but was present at high elevation zones of the Otter Creek sites. Woody biomass at plot 4 of Union Street was dominated by *Salix spp.* (willow), and site average dry mass of woody biomass was on the order of 362 (g dw m^{-2}), with stocks of woody biomass P around 0.27 ± 0.09 (g P m^{-2}). At Swamp Road, woody biomass was present at plots 3 and 4, and comprised of *Fraxinus pennsylvanica* (green ash), *Acer rubrum* (red maple), and *Acer saccharinum* (silver maple); site average dry matter stocks of woody biomass ~17,500 (g dw m^{-2}) and P stocks of woody biomass were ~13.1± 4.4 (g P m^{-2}). Results for live aboveground and belowground herbaceous biomass (collected in early September 2019) and P contents are shown in Table 5. Aboveground herbaceous biomass TP stock ranged from ~0.4 – 1.25 g P m^{-2} and was greatest at Union Street, followed by Swamp Road and then Prindle Road. The stocks of TP in belowground biomass (g P m^{-2}) were greatest at Union Street (2.20 ± 1.58), followed by Prindle Road at 1.31 ± 0.45, then Swamp Road at 1.03 ± 0.51.

5.2.4. Litterfall and Litter Decomposition

Litterfall production, collected in Fall 2019, was on average ~400 g dw m^{-2} y^{-1} and did not differ significantly between sites (Table 5). The corresponding P stocks (g P m^{-2}) at Prindle Road, Union Street, and Swamp Road were 0.6 ± 0.4, 0.47 ± 0.18, and 0.61 ± 0.32, respectively. For samples collected in Fall 2020, litterfall production (g dw m^{-2} y^{-1}) was 419 ± 220 at Prindle Road, 795 ± 324 at Union Street, and 559 ± 212 at Swamp Road, resulting in greater litter P stock estimates for the two Otter Creek sites in 2020 compared to 2019.

Figure 8 shows results from the litter decomposition experiment. Litterfall collected in 2019 was used to make litter bags which were incubated at the sampling plots for a maximum of 297, 351, and 354 days at Prindle Road, Union Street, and Swamp Road, respectively. The percent mass loss over that period was 56.1 ± 16%, 71.4 ± 20%, and 61.7 ± 14% at Prindle Road, Union Street, and Swamp Road, respectively. The cumulative mass (d.w.) losses over the incubation period equate to daily mass decay rates of -0.0026 ± 0.0078 d^{-1} at Prindle Road, -0.00118 ± 0.0035 d^{-1} at Union Street, and -0.00184 ± 0.0055 d^{-1} at Swamp Road.

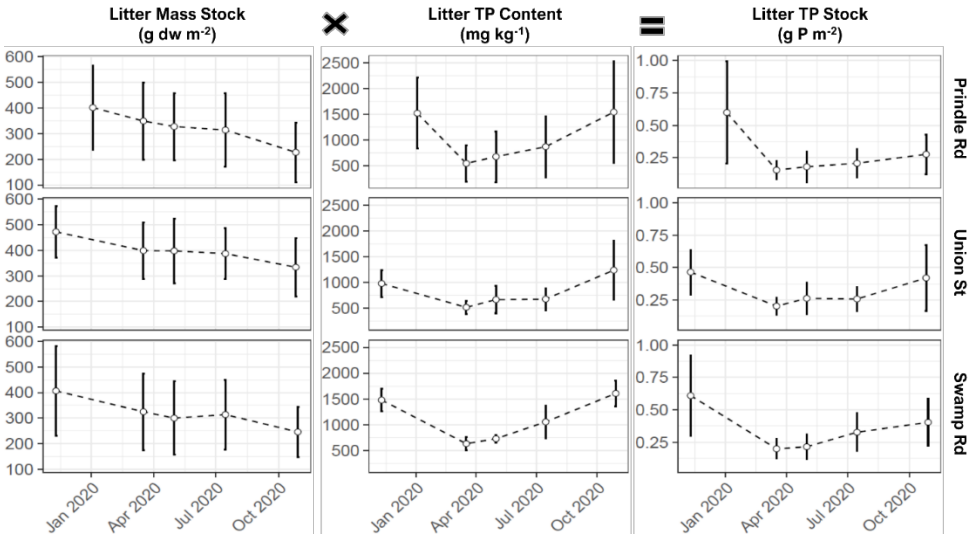

Figure 8. Site level averages for litter stocks over time estimated from the litterbag decomposition experiment, with (A) stock of dry mass, (B) total P content of litter, and (C) stock of total P. Error bars denote standard deviation.

The litter TP content (mg P kg^{-1}) decreased markedly over the first incubation period in the winter, then increased or stayed constant in each successive incubation period at each site (Figure 8). Final litter TP stocks were highest at Union Street, followed by Swamp Road, and Prindle Road. The ratio of HCl-P_i to HCl-TP for litterbags decreased on average at all sites from 0.55 ± 0.12 initially to 0.23 ± 0.09 at the end of the last incubation period, with HCl-Pi increasing relative to HCl-TP at higher elevation plots (multiple regression on HCl-[Pi:TP] vs. incubation time and depth: r^2 = 0.77, p = 0.008).

5.2.4. Accretion

Figure 9 shows rates of material accretion and P accretion as a function of the 90th percentile flooding depth for each sampling plot at each site.

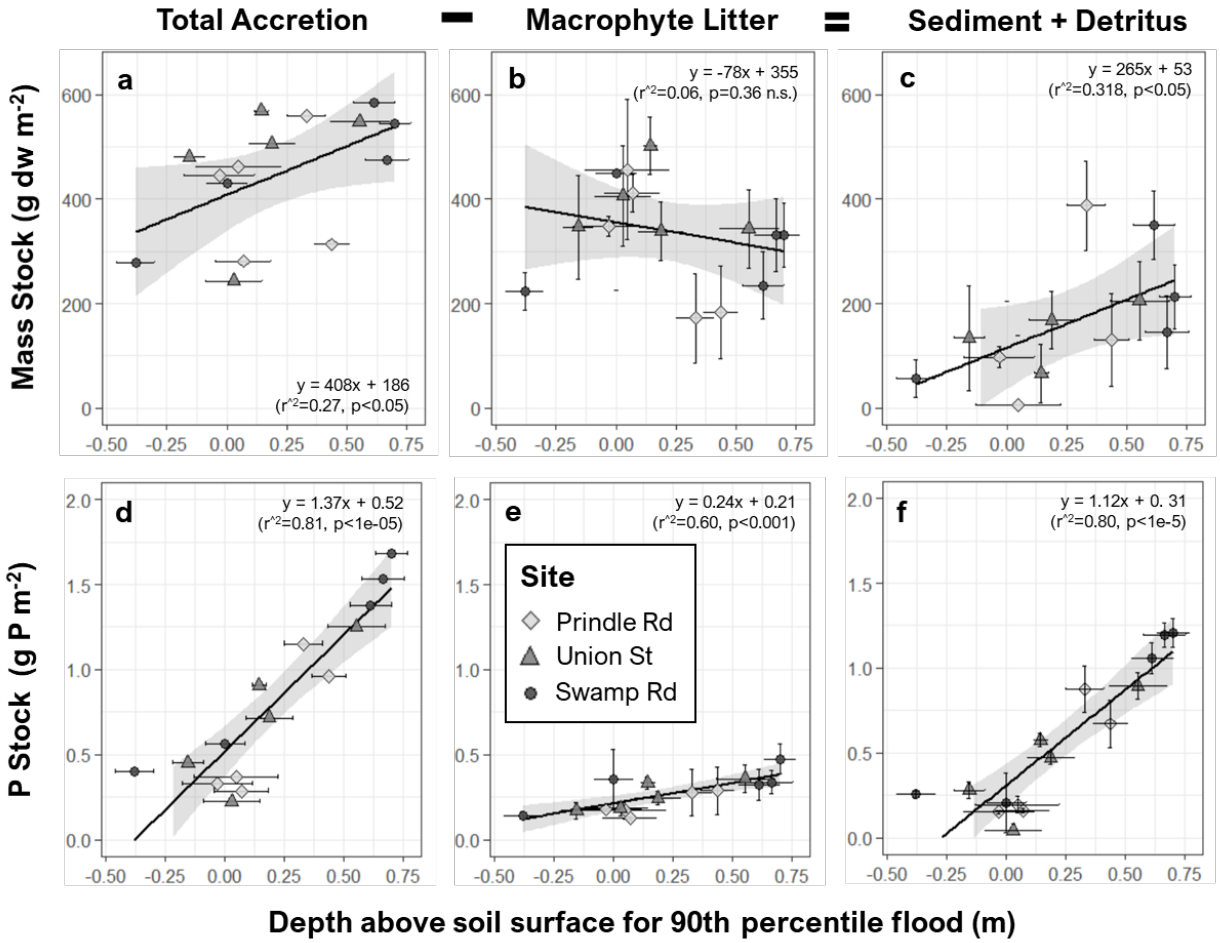

Figure 9. Accretion (including litter, sediment, detritus) over ceramic tiles plotted against water depth above soil surface for 90th percentile flood for each site, showing mass stocks (top row), P stocks (bottom row) for total accretion (a & d), macrophyte litter (b & e), and sediment and detritus (c & f). Sediment + detritus is calculated as the difference between total accretion and macrophyte litter. Bars around points indicate standard deviation. Black lines and shaded areas show best fit lines for regressions, fit statistics are given on the top right of each sub-plot.

Mass accretion rates ranged from 200 to 600 g dw m^{-2} and were positively correlated with flooding depth (Figure 9a, $r^2 = 0.27$, $p < 0.05$). Herbaceous plant litter made up a substantial fraction of accreted mass at 180 – 500 g dw m^{-2} and was not significantly correlated with flooding depth (Figure 9b, $r^2 = 0.06$, $p = 0.36$). The mass of sediment and detritus – estimated as the difference between total accretion and litter – ranged from 0 to 400 g dw m^{-2} and was positively correlated with flooding depth (Figure 9**Error! Reference source not found.**c, $r^2 = 0.31$, $p < 0.05$). The rate of total P accretion ranged from 0.25 to 1.7 g P m^{-2} was highly and positively correlated with flooding depth (Figure 9d, $r^2 = 0.81$, $p <$ 1e-5). Macrophyte litter P in accreted material, ranging from 0.1 to 0.5 (g P m^{-2}), was positively correlated with flooding depth (Figure 9e, $r^2 = 0.6$, $p <$ 0.001), but it made up a relatively small amount of total P accretion. By subtracting macrophyte from total P accretion, we estimate P in accumulated sediment and detritus (periphyton, invertebrates, etc.) (Figure 9f). Sediment and detritus made up most of the stock of total P in accreted material (0 – 1.25 g P m^{-2}) and was highly and positively correlated with flooding depth (Figure 9f, $r^2 = 0.80$, $p <$ 1e-5). Inorganic mass accretion ranged from 50 to 200 g dw m^{-2} and was well correlated with flooding depth (Figure 10b, $r^2 = 0.48$, $p < 0.01$).

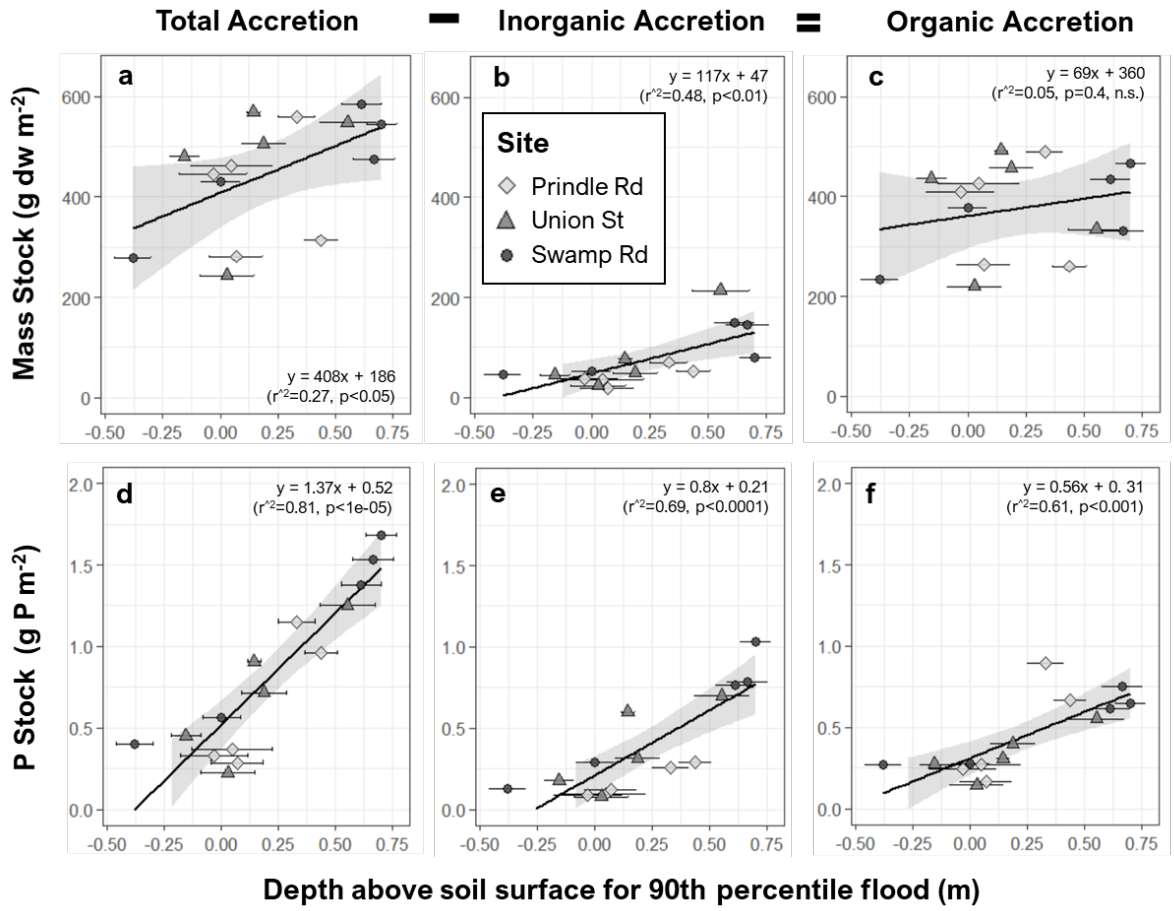

Figure 10. Accretion (including litter, sediment, detritus) over ceramic tiles plotted against water depth above soil surface for 90th percentile flood for each site, showing mass stocks (top row), P stocks (bottom row) for total accretion (a & d), inorganic accretion (b & e) and organic accretion (c & f). Organic accretion is calculated as the difference between total and inorganic accretion. Bars around points indicate standard deviation. Black lines and shaded areas show best fit lines for regressions, fit statistics are given on the top right of each sub-plot.

Organic matter accretion ranged from 200 – 500 g dw m^{-2} and was not correlated with flooding depth (Figure 10**Error! Reference source not found.**c, $r^2 = 0.05$, $p = 0.4$). Despite having similar magnitudes, accretion rates of organic matter and macrophyte litter were not correlated ($r^2 = 0.01$, $p = 0.66$). Organic P accretion was calculated from the difference between total P accretion (HCl-TP) and inorganic P accretion (HCl-P_i). Both inorganic and organic P accretion had similar magnitudes, 0.05 – 1.1 and 0.2 – 1 g P m^{-2}, respectively, and were positively correlated with flooding depth (Figure 10e and f, $r^2 = \sim 0.6\text{-}0.7$, $p < 0.0001$).

In another recent LCBP-funded project, Diehl et al. (2021) observed annual floodplain P deposition rates ranging from less than 1.0 g P m^{-2} y^{-1} to more than 100 g P m^{-2} y^{-1}. Our results in Figures 9 and 10 suggest that our three sites likely fall on the lower end of the P deposition spectrum presented by Diehl et al. (2021) for floodplains within the Lake Champlain Basin.

5.2.5. Water Monitoring during Flood Events

We collected a total of 522 grab samples that were analyzed for SRP and had valid YSI readings. Of those, 448 were analyzed for TP and 329 were analyzed for TSS. Figure 11 summarizes DO, SRP, TP and TSS concentrations observed at each site and uses a compact letter display to denote significant differences (alpha=0.05) within sites between groups of condition (filling vs. draining) and sample origin (inflow, river, wetland, outflow).

At Prindle Road, DO (mg L^{-1}) was greatest at the outflow during the filling condition and DO was not significantly different between the inflow and wetland. SRP at Prindle Road was greatest at the inflow, followed by the wetland then the outflow. TP and TSS at Prindle Road did not differ significantly between the inflow, wetland, and outflow, with the exception filling outflow samples, which had lower TP and higher TSS than other groups (Figure 11). At both Otter Creek sites, Union Street and Swamp Road, there were significant differences between the river and wetland with DO being higher in the river, SRP being lower in the river, TP being lower in the river, and TSS being higher in the river (Figure 11). In the wetlands of the Otter Creek sites, DO, TP, TSS, and (for Swamp Road only) SRP were significantly greater on the rising limb of floods when the floodplain was filling with river water than on the falling limb when wetlands were draining to the river (Figure 11). The river at both Otter Creek sites had higher TSS and TP on the rising limb (river filling wetlands) compared to the falling limb (wetlands draining to the river), while differences in river DO and SRP between limbs were not significant (Figure 11).

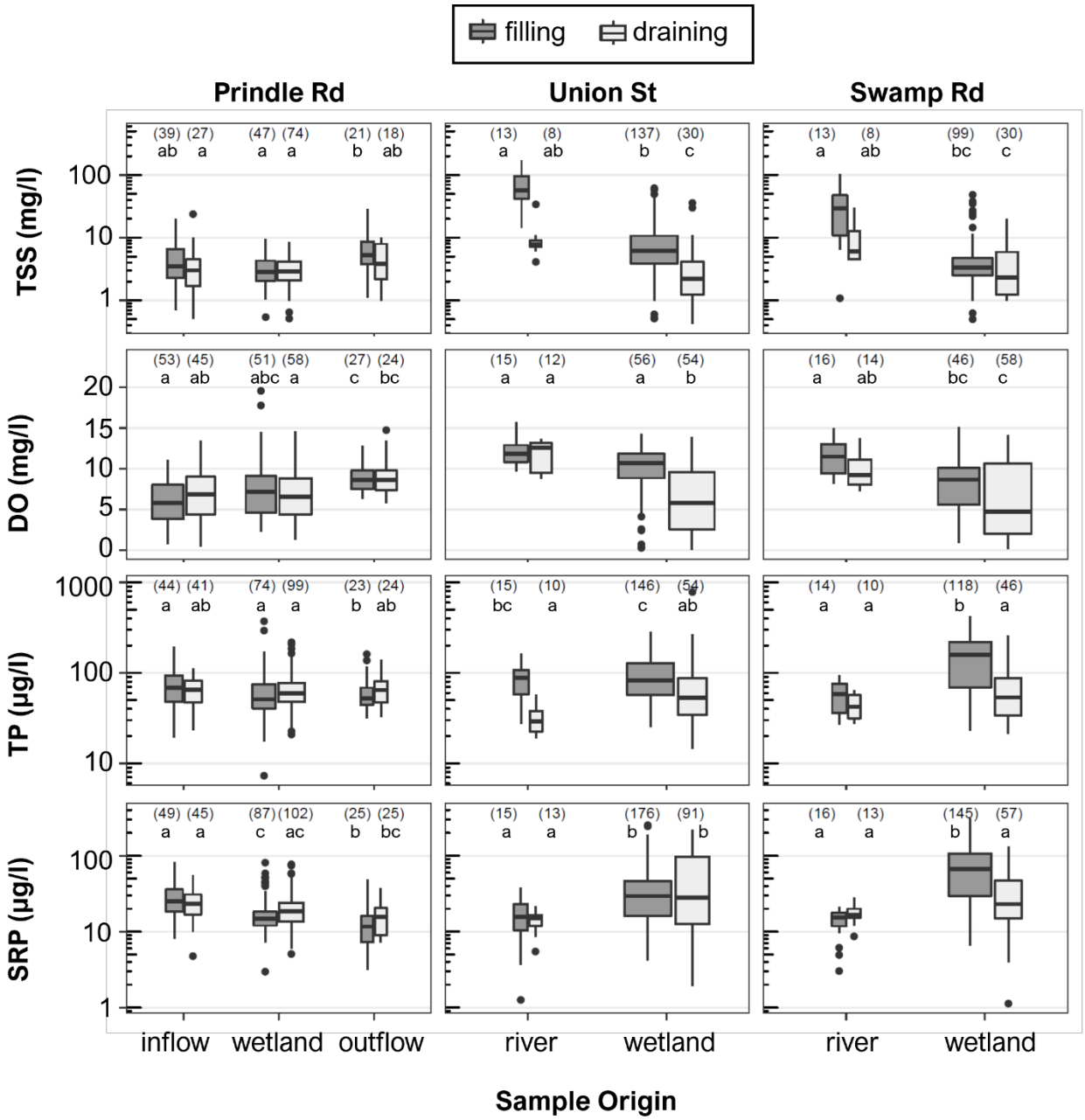

Figure 11. Panel showing box-and-whisker plots of concentrations of total suspended solids (TSS), dissolved oxygen (DO), TP, and SRP, in grab samples at each site. Shading of boxes denotes the condition of the system when samples were collected, dark grey for filling (water level rising) and white for draining (water level falling). The number of observations is given in parentheses above each group. Letters denote significant differences among groups (origin and condition) within sites (Dunn-Bonferroni, alpha = 0.05).

In the wetlands of Otter Creek sites and in samples of any origin at Prindle Road, TSS was a poor predictor of variability in TP. In these areas, there was weak correlation and heteroskedasticity in the TSS-TP relationship (Figure 12a). Conversely, TP was explained well by TSS in river samples of both Otter Creek sites: Union Street river samples had a very strong linear TSS-TP relationship (r^2 = 0.82, n = 20, p = 5.2e-8) and Swamp Road river samples had a strong linear TSS-TP relationship (r^2 = 0.63, n = 21, p = 1.8e-5) (Figure 12b and 12c). The inorganic fraction of TSS

was ~80% in the river at Otter Creek sites and ~50% at Otter Creek wetlands and at Prindle Road. In the Otter Creek wetlands and the inflow of Prindle Road, variability in TP was explained by SRP well at higher concentrations (SRP > 0.05 mg P L^{-1}), where TP increased ~1:1 with SRP, and less well when was SRP below 0.05 mg P L^{-1}) where the TP-SRP slope tended to be greater than 1:1 (Figure 13). At the wetland and outflow of Prindle Road, the variability in TP was poorly explained by both SRP and TSS (Figure 12, Figure 13). At all three sites, SRP was significantly related to DO according to a negative exponential model. This relationship was strongest at Swamp Road, followed by Union Street, then Prindle Road (Figure 14).

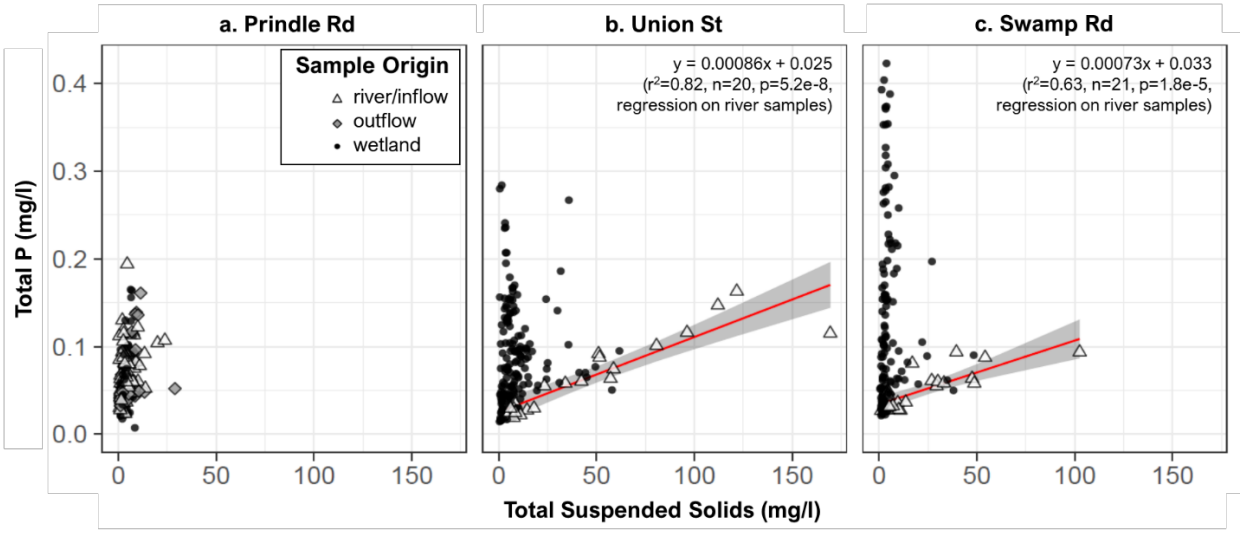

Figure 12. Scatterplot of TSS and TP in grab samples taken at each sample site: Prindle Road (a, left), Union Street (b, center), and Swamp Road (c, right). Shapes correspond to sample origin: river/inflow (white triangles), outflow (grey diamonds), and wetland (black circles). The red line shows the best fit regression line and the shaded grey area shows the 95% confidence interval for the best fit line. Model fits are shown for river samples at Union Street and Swamp Road fit statistics are given on the upper right.

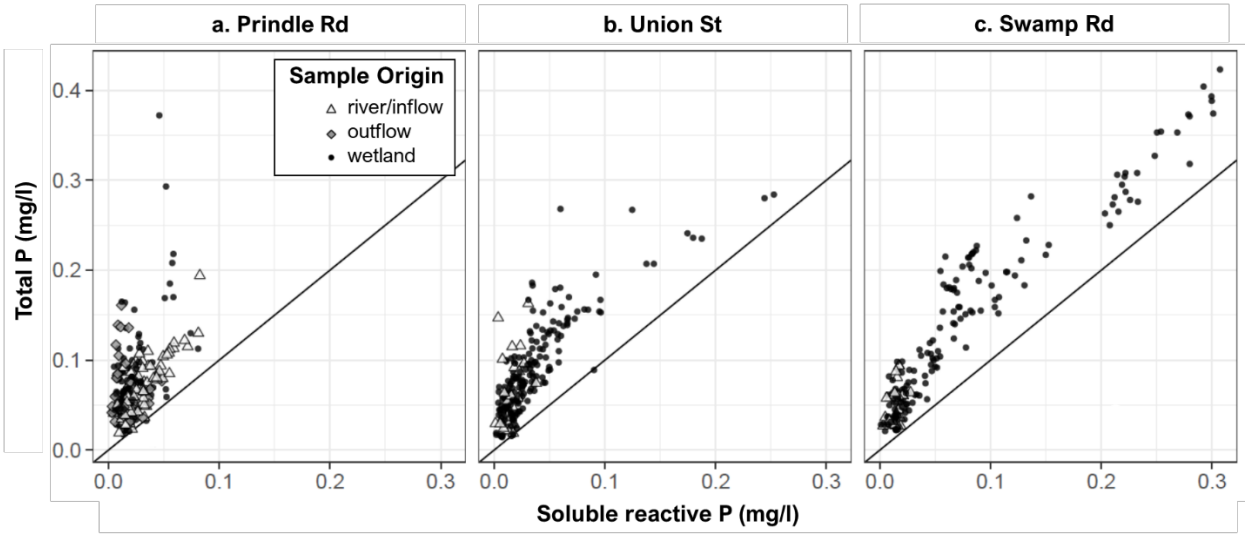

Figure 13. Scatterplot of TP and SRP water samples (including grabs, siphons, and ISCOs) taken at each sample site: Prindle Road (a, left), Union Street (b, center), and Swamp Road (c, right). Shapes correspond to sample origin: river/inflow (white triangles), outflow (grey diamonds), and wetland (black circles). The black line shows the 1:1 line.

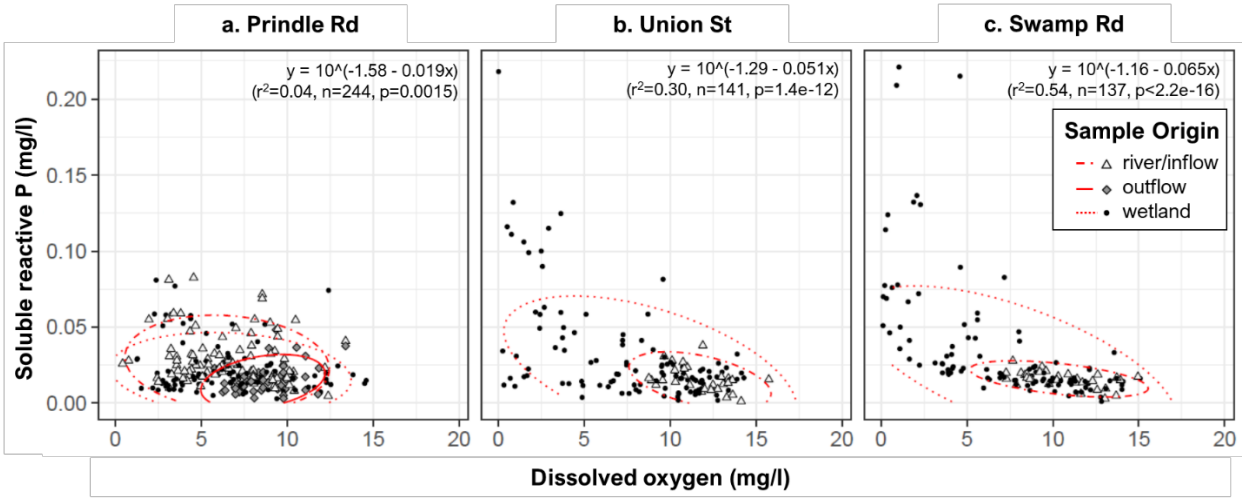

Figure 14. Scatterplot of DO and SRP in grab samples taken at each sample site: Prindle Road (a, left), Union Street (b, center), and Swamp Road (c, right). Shapes correspond to sample origin: river/inflow (white triangles, dot-dash ellipse), outflow (grey diamonds, solid ellipse), and wetland (black circles, dotted ellipse). Red ellipses are plotted to show differences in clusters between sample origins. Log-linear regression fit statistics of SRP vs DO are given on the upper right for each site.

Figure 15 below shows high frequency sensor data, along with SRP, TP, and TSS concentrations in the wetland water column at each site for three individual flood pulses that occurred in unique combinations in each watershed. SRP, TP, and TSS concentration data in Figure 15 come from samples collected using a combination of ISCO autosamplers and grab sampling to span the rising and falling limbs of each flood pulse.

In the Lewis Creek watershed, we captured a first flood pulse event at Prindle Road in late October of 2019. For this event, the water levels peaked near ~20cm above the median elevation plot, temperature ranged from ~5 to ~15°C, and DO ranged from ~20% to ~80% (Figure 15 R1, C1). Due to drought conditions in 2020, we moved the ISCO at Prindle Road from the median elevation plot (plot=2) to the lowest elevation plot (plot=0), and subsequently captured two more flood pulse events in 2021. One snow melt driven event occurred in March 2021, with peak depth (relative to plot 0) of ~32cm, temperature ranging from ~0°C to ~12°C, and DO ranging from ~20% to ~100% (Figure 15 R1, C2). Another rain driven pulse came in late-April/early-May 2021, with peak depth of ~45cm (relative to plot 0), temperature ranging from ~7 to 15°C, and DO ranging from ~0% to over 100% (Figure 15 R1, C3). Each of the flood pulses captured at Prindle Brook corresponded to a discharge event on the Lewis Creek lesser in magnitude than an AEP 50% event (2-year Recurrence Interval), as detailed in Appendix B.

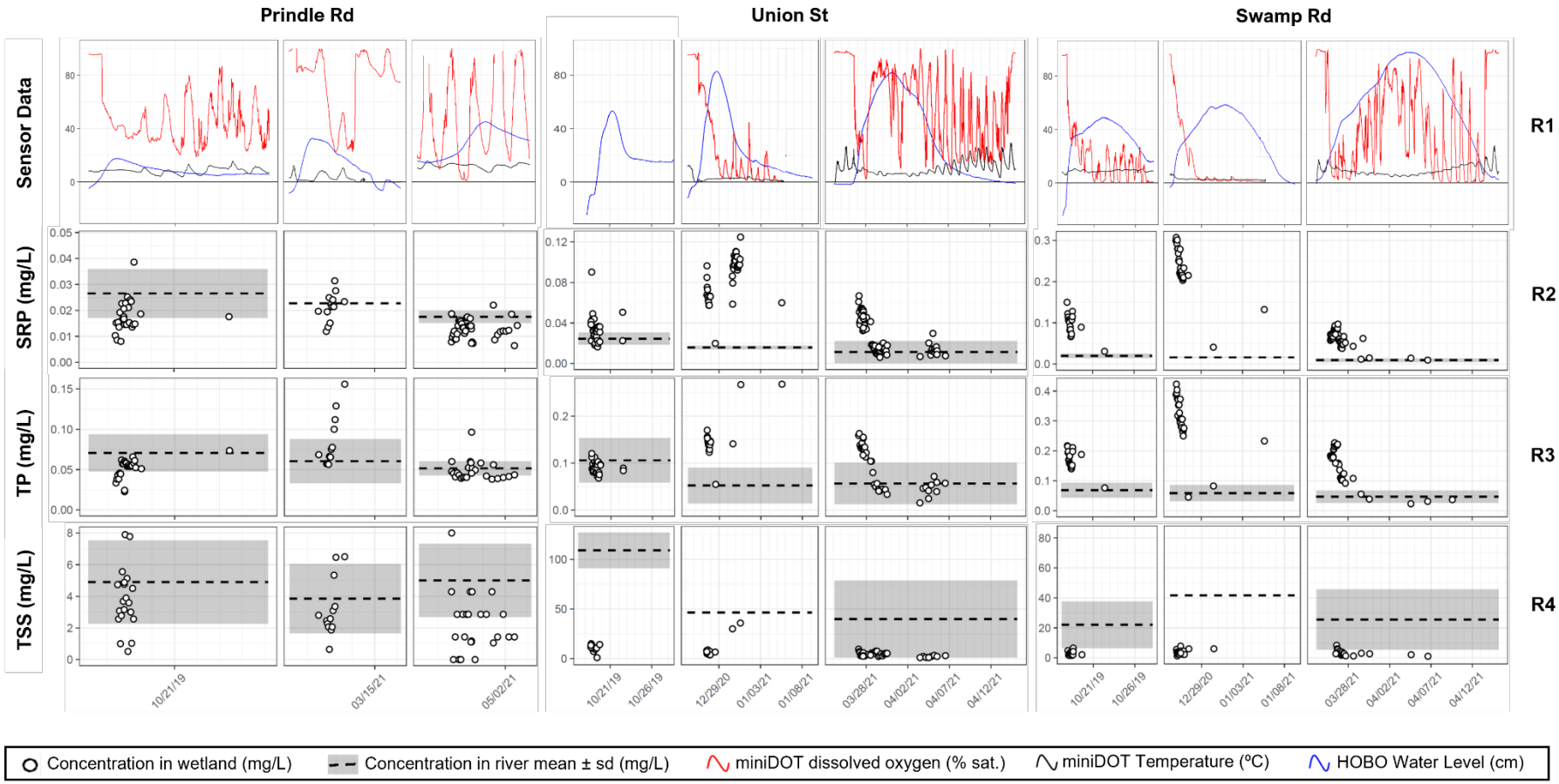

Figure 15. High frequency sensor data including water level, dissolved oxygen, and temperature (R1), and concentrations of SRP (R2), TP (R3), TSS (R4) at Prinde Rd (C1-C3), Union St (C4-C6), and Swamp Rd (C7-C9). Points show values measured in each wetland, while dashed lines and shaded areas show the mean and standard deviation, respectively, of the river concentrations for each pulse.

All data for Union Street and Swamp Road in Figure 15 correspond with the median elevation plot at each site (plot 2). The first event captured in Otter Creek was the same rain driven event in late October 2019 that occurred at the Prindle Road site. For this event, Union Street had a peak depth of ~55cm on 10/21, there was a power failure for the miniDOT sensor at Union Street, and therefore no data were collected for temperature and DO at the soil-water interface (Figure 15 R1, C4). At Swamp Road, the late October flood pulse produced a peak depth of ~45cm, temperature was consistently near 10°C, while DO dropped from 100% initially to 0% after 4 days then DO fluctuated between 0% and 30% for the remainder of the pulse (Figure 15 R1, C7). The second pulse captured in Otter Creek was a snowmelt and rain driven event that began on December 26th 2020; this event was preceded by six months of drought in the region (Heim & Sanchez-Lugo 2021). For this event, Union Street had a peak depth of ~85cm on 12/28/21, temperature was flat near ~2°C, and DO fell from 75% to 0% over three days then fluctuated between ~0% and 40% for the remainder of the event (Figure 15 R1, C5). At Swamp Road the peak flood depth was ~60cm on 1/1/21, temperature was flat near ~2°C, and DO fell from 95% initially to 0% after ~3.5 days and then ranged from 0%-10% for the remainder of the pulse (Figure 15 R1, C8). The third event captured in Otter Creek was driven by rain and mountain snowmelt that began on March 25 of 2021. At Union Street, the peak depth was ~80cm on 3/31/21, temperature ranged from 6°C to 20°C, and DO started at 95% then dropped to ~10% after three days then rose to ~80% and remained above 50% for most of the rest of the pulse (Figure 15 R1, C6). Meanwhile, at Swamp Road, the flood peak occurred on 4/5/21 with a depth of ~95cm, temperature ranged from 6°C to 20°C, and DO initially declined from 95% to 0% over the first 4 days then increased to above ~20% but below ~90% for about 1 week then declined to 0% and fluctuated between ~0% and ~80% for the remainder of the flood (Figure 15 R1, C9). All but one of the recorded inundation events at these Otter Creek sites were referenced to peak discharge values at the nearby USGS gages lesser in magnitude than an AEP 50% event (2-year RI). The December 2020 event corresponded to an approximate AEP 50% event at the Otter Creek Center Rutland gage (Appendix B).

Figure 15 shows concentrations observed in the wetland water column of the ISCO sampling plot as white circles for SRP (row 2), TP (row 3), and TSS (row 4). Dashed black lines and shaded areas in Figure 15 represent the respective mean concentration of the river grab samples for a given flood pulse. At Prindle Road, the concentrations of SRP, TP and TSS in floodwater on the wetland ranged from ~0.01 to 0.04 mg SRP L^{-1}, 0.02 to 0.16 mg TP L^{-1}, and 0 to 8 mg TSS L^{-1}. Peak concentrations typically coincided with the peak water level and tended to be within or below the shaded area denoting river (i.e., stream) concentrations (Figure 15, R2-R4 and C1-C3). At Union Street, the SRP and TP concentrations ranged from 0.01 to 0.13 mg SRP L^{-1} and 0.01 to 0.27 mg TP L^{-1}. At Swamp Rd, SRP and TP concentrations ranged from 0.02 to 0.31 mg SRP L^{-1} and 0.02 to 0.42 mg TP L^{-1}. TP and SRP concentrations at Otter Creek sites followed similar patterns, tending to peak above levels observed in the river on the rising limb of the flood, then decline to near the levels predicted by the river at the crest and falling limb of floods. During the flood pulse beginning on 12/27/20, concentrations of TP and SRP at both Otter Creek sites remained above levels predicted by the river on both the rising and falling limbs of the pulse (Figure 15, R4 and C4-C9). At both Otter Creek sites, TSS concentrations in the wetlands were largely less than 20 mg TSS L^{-1} and consistently lower than concentrations measured in the river (Figure 15 R4 and C4-C9), thus providing evidence that river suspended solids were being captured on site.

These high-resolution data reveal several important dynamics relevant to riparian wetland P cycling. In many cases, diurnal oscillations in DO and temperature occurred within flood water ~5 cm above the sediment-water interface in many cases, with both measures commonly reaching daily maximums in late afternoons and daily minimums in early mornings. These patterns in DO suggest photosynthesis-respiration dynamics common for shallow water bodies. These data also suggest that our "aerobic" intact core experiments in the laboratory, where room air was bubbled into core water columns 1-2 hours per day for reaeration and then turned off allowing DO declines due to sediment oxygen demand until reaeration the following day, better represent reality than when more fully anaerobic conditions were imposed using N_2 gas. The exceptions were winter floods (middle column for each site in Figure 15), when DO remained depressed during the majority of the flood pulse, which was likely caused by the inhibition of photosynthesis in the water column by low temperatures. Our grab sampling data suggest that elevated SRP concentrations correspond with lower DO in the Otter Creek wetlands (Figure 14). Therefore, winter flood pulses with less primary productivity may result in prolonged anaerobic conditions and increased internal SRP loading to the water column from soils. Furthermore, less SRP will be assimilated into plant biomass (including macrophytes, periphyton, and phytoplankton) during these cold flood pulses, also potentially contributing to elevated water column SRP. Seasonal flow duration curves from Otter sites show slightly higher magnitude of low-frequency (Qp99) events occurring in winter months (Dec-Jan-Feb) (Appendix B). This could possibly due to more rain instead of snow, more rain-on-snow events, and earlier thaw events (Hodgkins and Dudley, 2006; Dudley et al., 2017), and could potentially create higher risk of SRP loss from riparian wetlands.

It is also interesting to note that we generally observed the greatest SRP concentrations at our Otter Creek sites early in the flood pulses. Our laboratory incubations suggest that diffusive flux of SRP reaches maximum (i.e., equilibrium) SRP concentrations after ~1 week. However, our field data suggest maximum SRP concentrations in the water column occur more quickly during flood pulses. We hypothesize that this is due to rapid mineralization of organic material on top of and within surface soils, along with the liberation of very loosely held inorganic P, upon initial rewetting (Gu et al., 2018; Schönbrunner et al., 2012; Sigua et al., 2009; Surridge et al., 2012). Further, it seems likely that river water having lower SRP concentrations then provides a dilution effect at the peak of the flood pulse, after which SRP diffusion from soils can continue to occur as evidenced by the winter flood pulse dynamics we observed (Figure 15 C5 and C8), but SRP concentrations in the water column might stay suppressed during warmer periods due to biological assimilation of SRP (Figure 15 C6 and C9). More research is needed to enhance understanding of the role of biology (especially periphyton) in suppressing internal loading of SRP from soils during flood pulses.

5.3. Model Calibration & Scenarios

5.3.1. Model Calibration and Verification

Our calibration, and verification was focused on estimating likely values for stochastic parameters. First, we set a range for stochastic parameter values based on the literature and, where-possible, statistical fits to direct measurements we made in the lab or field during this project (Appendix C). Next, we estimated a likely range of the parameters that were not directly measured using a series of hierarchical tests involving systems of increasing complexity. We first calibrated the value of parameters affecting soil water SRP fluxes (adsorption and diffusion) by simulating intact soil core

experiments corresponding to data presented in Figure 7 in Section 5.2.2 (also see Appendix C). Then we investigated assumptions and calibrated model parameters by verifying performance against inorganic accretion data, biomass, and litter stocks (in that order) from our three field sites using the first year of field data (7/15/19 – 7/15/20) (Appendix C).

The following Wetland P Model calibration criteria were met using the first year of field data:

1. Biomass (d.w.), inorganic sediment deposition (d.w), litter P (d.w.), were all clustered near the 1:1 line for modeled versus measured results and modeled results had approximately the same mean and variance as observations (when data was pooled across all sites and plots)
2. Water column DIP (i.e., SRP) and total P stocks (g/m^2) were within the same order of magnitude observed in the field during floods and modeled results had roughly the same mean and variance as observations (when data was pooled across all sites and plots)
3. Stocks of soil organic matter were relatively stable (not increasing or decreasing by more than 1 – 2% per year).

The model was verified with field data from year two using the criteria above, except for litter P (data unavailable).

Important parameters in the Wetland P Model include hydraulic retention time (HRT), water level, and influent water quality (specifically concentrations of TSS, TP, and SRP). We utilized an existing 2D HEC-RAS model for Otter Creek (Trueheart, 2019) to determine the relationship between water level and HRT at Union Street and Swamp Road for flood inundation depths of ~1-2 m. HRT data generated from the HEC-RAS model were well predicted by negative power law models using water elevation (Figure 16). For the Prindle Road site, we calculated HRT based on water volume (estimated by water level measurements and site DEMs) and measured system outflow (Figure 17). Changes in the relationship between HRT and wetland water level over time were evident, which we assume were caused by changes in the beaver dam controlling outflow. See Appendix C for more details.

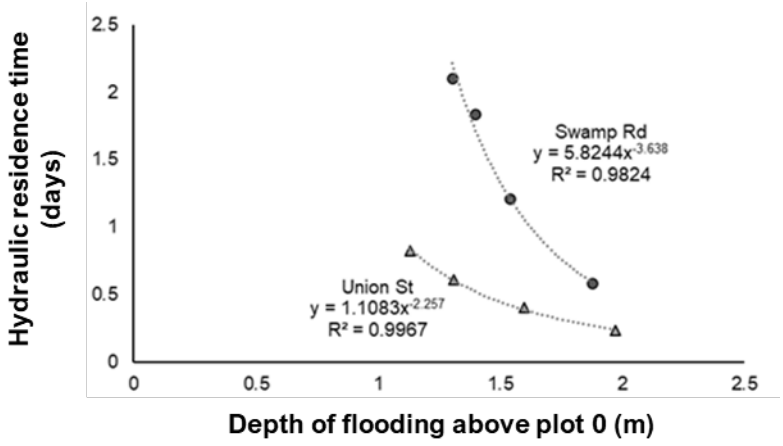

Figure 16. Relationship between depth of flooding and floodplain hydraulic residence time predicted for the two Otter Creek riparian wetland sites using a 2D HEC-RAS model for Otter Creek (Trueheart, 2019).

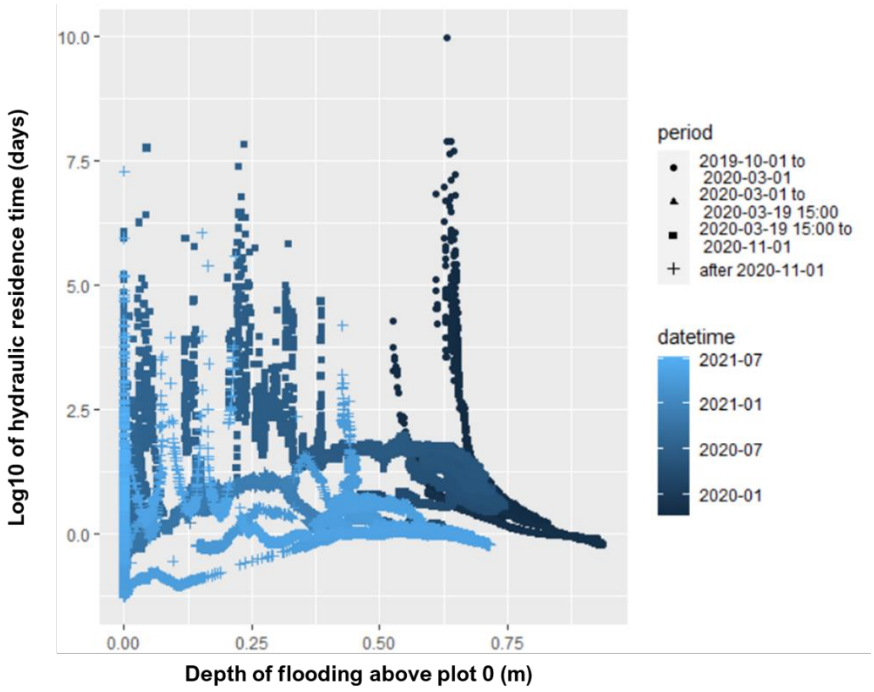

Figure 17. Relationship between depth of flooding in meters and hydraulic residence time based on system volume and outflow as estimated by field measurements for the Prindle Road site. Different colors represent three distinct phases of apparent beaver dam influence during the monitoring period.

Based on the relationships shown in Figures 16 and 17, we determined negative power law equations to predict HRT based on water elevation for each site that represent extrapolations of the observed relationships (Figure 18) due to the fact that most of the water levels observed during our field monitoring were in the vicinity of ~0.5 m. We also decided to run some model scenarios assuming constant HRTs of 10 or 100 days, in addition to simulations using the negative power law models.

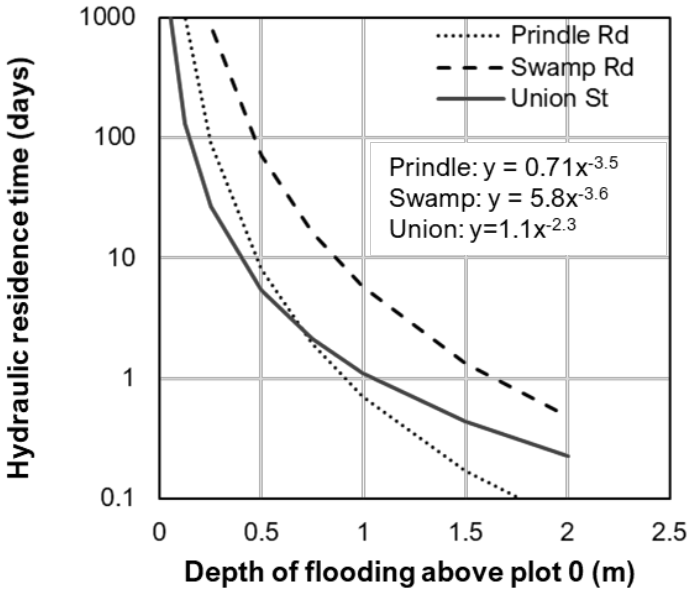

Figure 18. Negative power law models for hydraulic residence time as a function of water elevation relative to low elevation plot surface (plot 0) for the three study sites.

In order to contextualize our observed flood pulse events and modeled scenarios that included changes in flood pulse wetland water levels, we analyzed flow duration curves for Otter Creek and Lewis Creek and determined trends for wetland inundating flows (see results in Appendix B).

To estimate influent water chemistry for model simulations, we analyzed field data for both passive siphon samplers (Figure 19) and stream (i.e., river) grab samples (Figure 20) collected during the course of the project. For each group of samples, we determined the organic fraction of TSS and the SRP fraction of TP, which we used to estimate inputs of organic P, dissolved inorganic P, and particulate inorganic P to the control volume during modeling. We evaluated model simulations that assume 100% particle retention within the wetland, which appears to be a reasonable assumption based on the low TSS concentrations (0-3 mg/L) measured in the wetlands towards the later periods of flood pulses (Figure 15), as well as those where particle settling is modeled and thus particulate export from the system is possible. For the simulations including the particle settling model, settling velocity was estimated based on particle density and radius, with particle density based on soil texture for inorganics and literature values for organics (Marois & Mitsch, 2016).

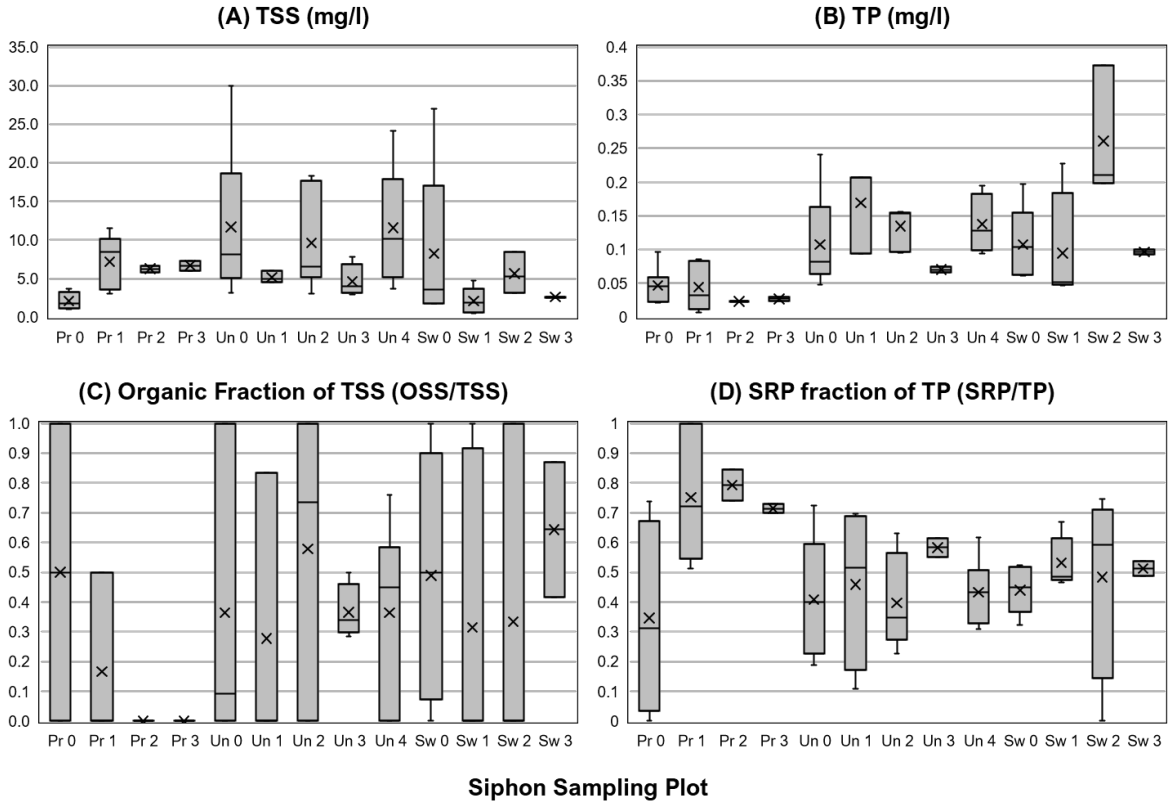

Figure 19. Box and whisker plots showing concentrations measured in rising limb passive siphons placed at each sampling plot for all three monitored flood events. Median concentrations are marked by horizontal lines in the middle of each box. Mean concentrations are shown as x's. Pr = Prindle Road, Un = Union Street, Sw = Swamp Road.

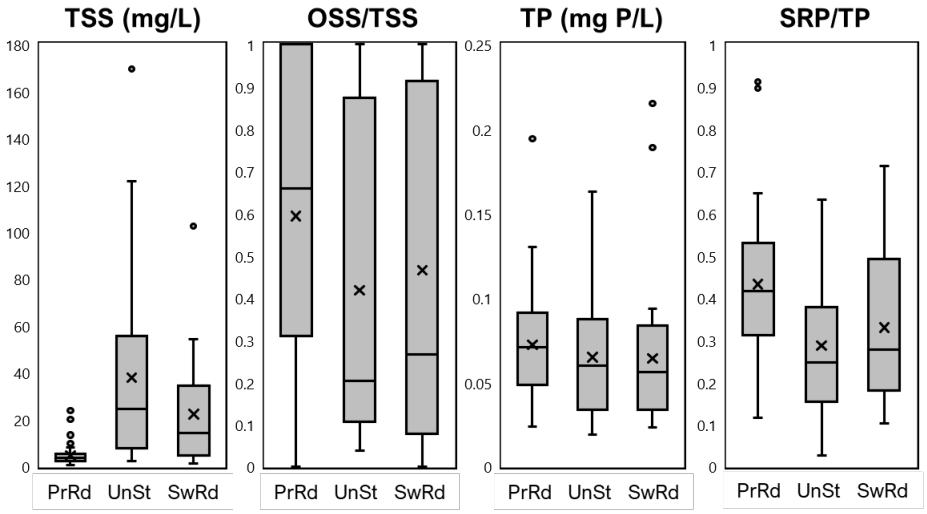

Figure 20. Box and whisker plots showing concentrations measured in the stream or inflow locations of each site. Median concentrations are marked by horizontal lines in the middle of each box. Mean concentrations are shown as x's. PrRd = Prindle Road, UnSt = Union Street, SwRd = Swamp Road.

5.3.2. Model Scenarios

We modeled scenarios as part of a sensitivity analysis. In this section, we present a series of figures showing how different factors affect net P retention (g P m^{-2} yr^{-1}) in the three riparian wetland sites studied in this project. All simulations were run for the two-year field monitoring period. First, we tested the model using influent TSS and P concentrations based on passive siphon samples versus stream (i.e., river) grab samples across a range of HRT assumptions (power model, fixed at 100 days, or fixed at 10 days) for the median elevation plot at each site (Figure 21).

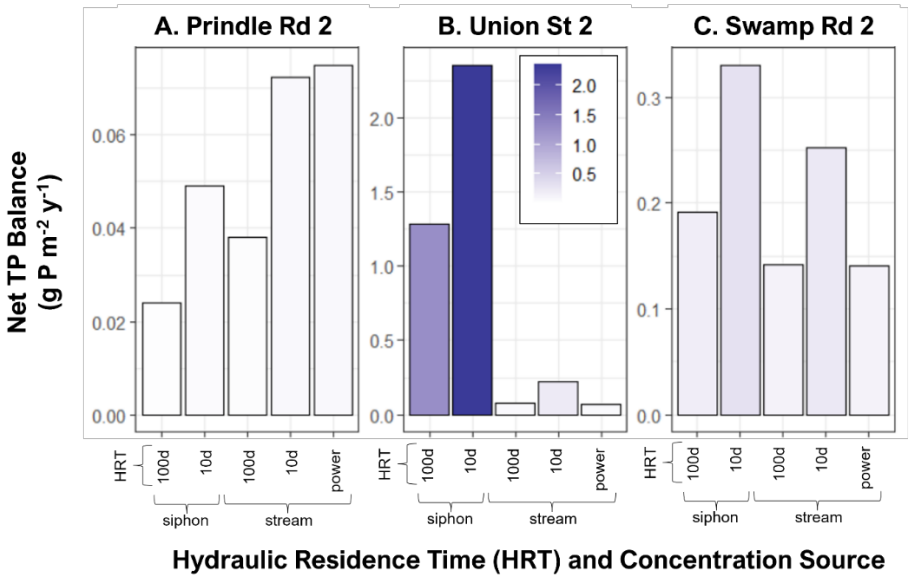

Figure 21. Annual net total phosphorus (TP) balance for 2-yr simulations of scenarios having differences in inflow P and TSS concentrations and hydraulic residence time (HRT) at the median elevation plot for each site. For each combination of inflow P concentrations, HRT was simulated as 100 days, 10 days, and using the negative power law relationships. From left to right, inflow concentrations are passive siphon data from the plots and stream (i.e., river) concentrations. The Y-axis scales is different for each site to show differences in scenarios. The color scale is for Net TP Balance and applies to panels A, B, and C.

Results from these simulations show that using passive siphon data instead of the stream concentrations has the largest impact for the Swamp Road site, resulting in an order of magnitude increase in net P retention (up to 2.7 g P m^{-2} yr^{-1}). This difference is caused by the relatively high SRP concentrations observed in passive siphon samples collected at Swamp Road plot 2 during the rising limb of flood pulses (Figure 21). Greater SRP concentrations can decrease the SRP concentration gradient at the sediment-water interface and thereby restrict diffusion of SRP from soils to floodwater, leading to greater net P retention. Using stream concentrations instead for Swamp Road plot 2, which seems more likely to capture site-level dynamics, means assuming greater TSS in influent, which can increase P deposition, but also lower SRP in the water column, which can increase the SRP concentration gradient at the sediment-water interface and thereby increase internal loading from sediments. Furthermore, Swamp Road (and Prindle Road) soils exhibited greater SRP release during laboratory intact core incubations compared to Union Street, which was represented in the model using different assumptions for the equilibrium P concentration. Differences in net P retention results for siphon versus stream concentrations were much less pronounced for Union Street and Prindle Road. Figure 21 also illustrates the effect of HRT assumption for each site. Assuming shorter fixed 10-day HRT led to greater net P retention

compared to fixed 100 d HRT model runs for all site-influent combinations. Results using stream concentrations show that the power models for HRT (i.e., dynamic HRT predicted based on water level) produced very similar results to the fixed 10-day HRT scenario for Prindle Road, and to the fixed 100 day HRT scenarios for both Otter Creek sites. Overall, net P retention estimates ranged from approximately 0.02 to 2.7 g P m^{-2} yr^{-1} (0.2 to 24 lbs P $acre^{-1}$ yr^{-1}) for all scenarios shown in Figure 21, with the most realistic scenarios (stream concentrations, dynamic HRT based on power model) resulting in net P retention near 0.1 g P m^{-2} yr^{-1} (1 lb P $acre^{-1}$ yr^{-1}).

Next, we evaluated the effects of different assumptions concerning particle settling on net P retention estimates across 3 plots per site, assuming stream concentrations and dynamic HRT based on power models (Figure 22).

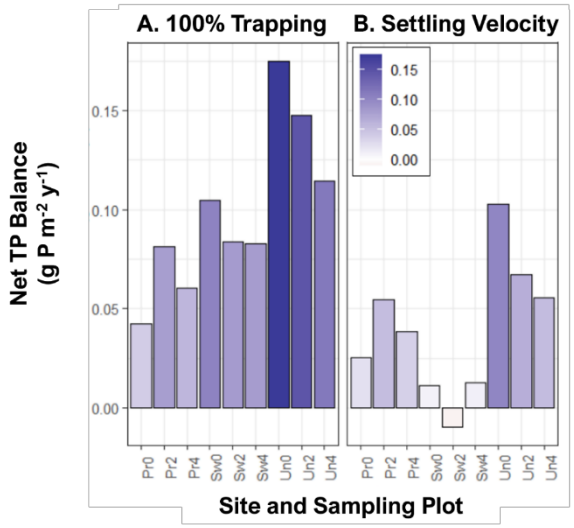

Figure 22. Annual net total phosphorus (TP) balance for 2-yr simulations of 3 plots per site under scenarios having differences in assumptions concerning particle trapping, with stream concentrations and dynamic HRT based on power models used in all cases. The color scale is for Net TP Balance and applies to panels A and B.

Assuming 100% particle trapping, which is reasonable for our sites most of the time (especially during low flow periods) based on the very low TSS concentrations observed in wetland floodwater during falling limb periods, resulted in net P retention values ranging from approximately 0.04 to 0.175 g P m^{-2} yr^{-1} (0.4 to 1.6 lbs P $acre^{-1}$ yr^{-1}). Modeling particle trapping based on settling velocity results in incomplete sediment retention at high flows, due to decreasing sediment retention efficiency as HRT declines in response to increasing water level. Simulations that modeled particle settling resulted in net P retention values ranging from slightly below 0 to ~ 0.1 g P m^{-2} yr^{-1} (-0.1 to 1 lbs P $acre^{-1}$ yr^{-1}) (Figure 22).

Net P retention in the Wetland P Model is the balance between P imports to and exports from the control volume. Figure 23 below shows imports (blue) and exports (red) on the basis of TP (circles) and SRP (X's, SRP = DIP) for various scenarios. For 100% particle trapping scenarios, all P export is SRP, whereas when particle trapping is estimated based on settling velocity some particulate P is also exported from the control volume. In all cases particulate P import is greater than particulate P export, while SRP import is always less than SRP export. Figure 23 also illustrates the strong effect of influent TSS and P concentrations on net P retenion. Greater influent concentrations of TSS and P lead to enhanced net P retention. For example, net P retention values ranged from <0 to 0.08 g P m^{-2} yr^{-1} (<0 to 0.7 lbs P $acre^{-1}$ yr^{-1}) and 0.1 to 0.3 g P m^{-2} yr^{-1} (0.9 to 2.7 lbs P $acre^{-1}$ yr^{-1}) for 0.5x median stream concentrations and 2x median stream concentrations, respectively.

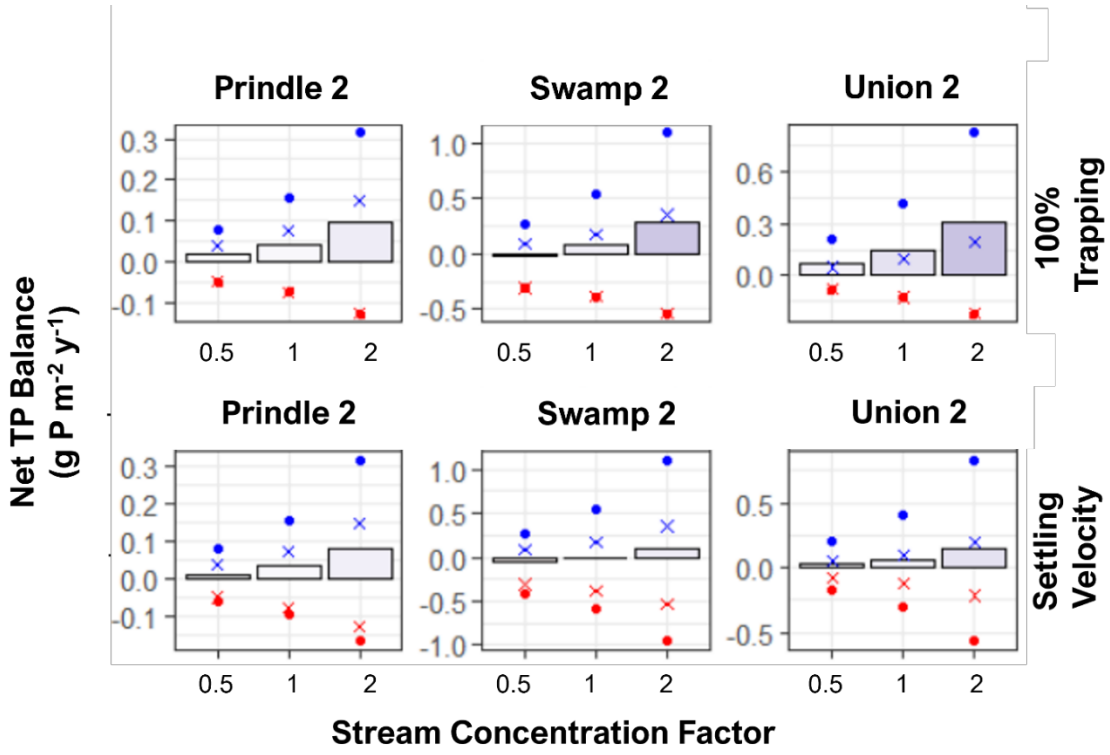

Figure 23. Simulated net total phosphorus (TP) balance (bars) with inflow P and TSS concentrations set to 0.5x stream (i.e., river) median, stream median, or 2x stream median for median elevation sampling plots in Prindle Rd (Pr), Swamp Rd (Sw), and Union St (Un) sites. Scenarios are shown having different assumptions about particle trapping (top row assumes 100%, bottom row simulates particle settling). P gains (blue) and P losses (red) on the basis of TP (circles) and SRP (X's, SRP=DIP) are also shown for various scenarios. HRT is assumed to be 100 days.

Finally, we investigated the effects of increasing flood magnitude on model estimates of net P retention by simulating scenarios where water levels forcing the model were multiplied by a factor of 1.2 (Figure 24). While our analysis of flow duration curves did not suggest a strong increasing trend in the frequency of inundation events, we decided to test greater water input using the power law models relating HRT to water level at each site. The factor of 1.2 is meant to represent a high-end estimate for increases in average flows in the next several decades to due to wetter climate in the Lake Champlain Basin (Guilbert et al., 2014). The model predicted that as more water moves through the wetland system control volume, there are minimal effects on net P retention at the scale of flow increases imposed (Figure 24). More floodwater leads to more P deposition, but also greater liberation and export of SRP. Combined, these dynamics lead to fairly stable net P retention estimates for a given set of influent concentration assumptions. To the contrary, Figure 24 again shows the pronounced effect of influent concentrations on net P retention, with far greater retention (up to 0.3 g P m^{-2} yr^{-1}) for high concentrations (2x stream medians) versus low concentrations (0.5x stream medians).

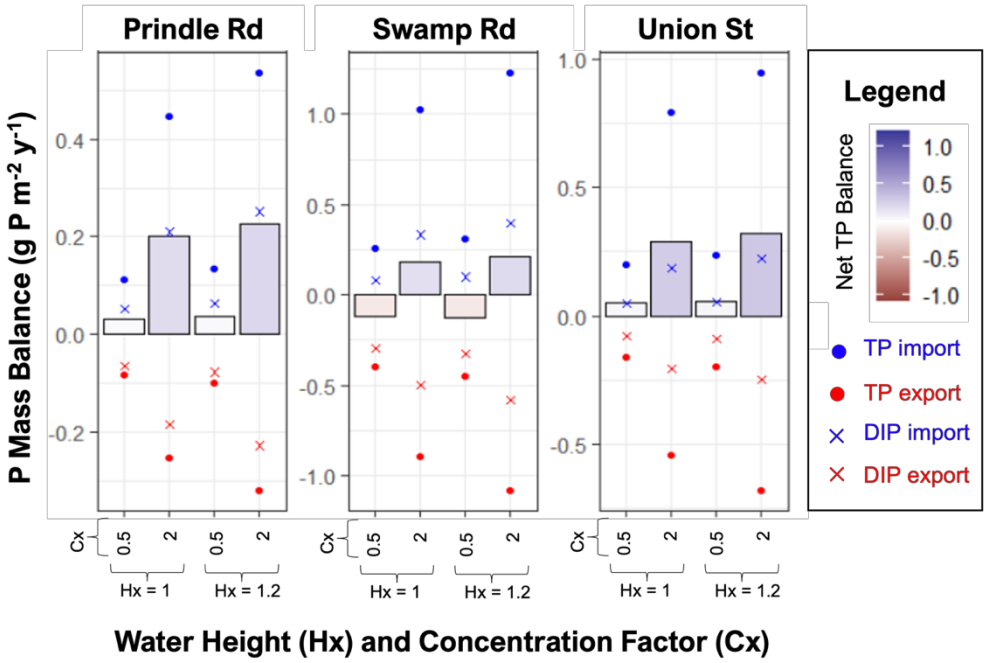

Figure 24. Simulated net total phosphorus (TP) balance (bars) with inflow P and TSS concentrations set to 0.5x stream (i.e., river) median or 2x stream median at observed (x1) and larger (x1.2) flood magnitudes for median elevation plots in Prindle Rd (Pr), Swamp Rd (Sw), and Union St (Un) sites. Particle trapping is estimated based on settling velocity. P gains (blue) and P losses (red) on the basis of TP (circles) and SRP (X's, SRP=DIP) are also shown for various scenarios. HRT is dynamic based on site-specific power models.

Figure 25 summarizes hydrologic and biogeochemical controls on P retention, comparing net P retention for siphon data, and multiple stream concentrations at HRT values of 10 and 100 days. Results shown in Figure 25 suggest that biogeochemical and hydrologic forces are both important. They also indicate that if efforts to decrease P loading from agricultural and urban land are successful in the future and result in reduced riverine P concentrations (e.g., decreasing by a percentage similar to the 34% load reduction required by the TMDL; U.S. EPA, 2016), this could decrease the magnitude of P retention possible for riparian wetland systems.

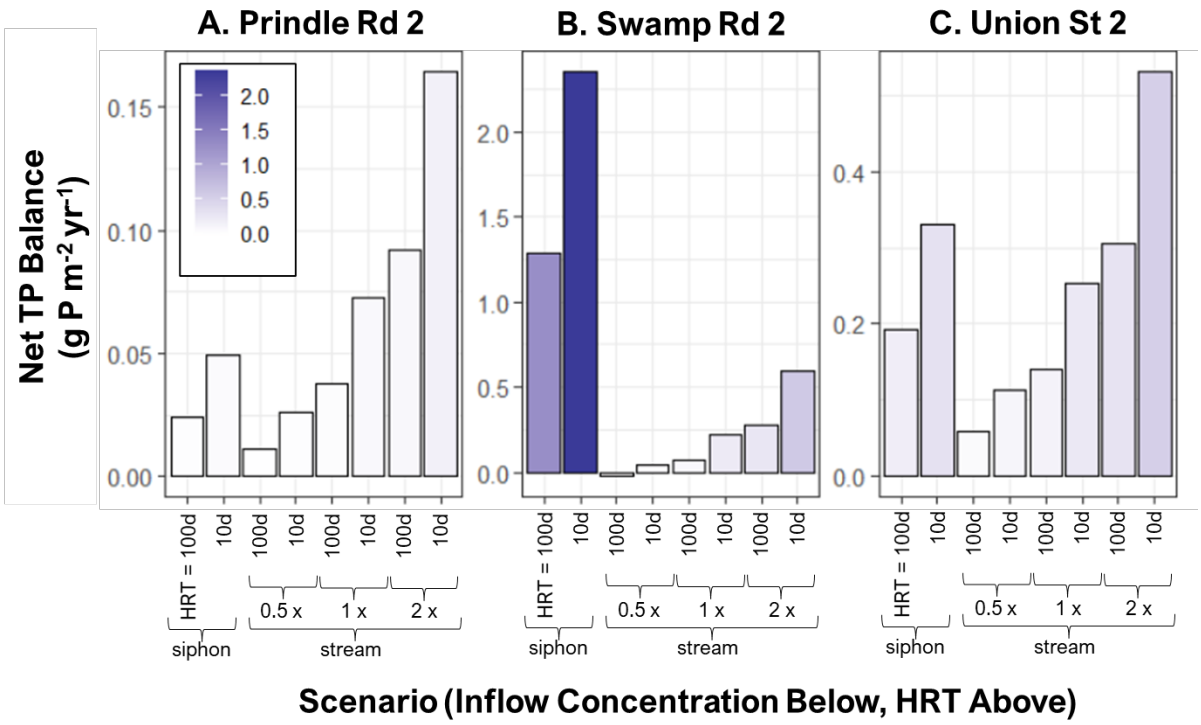

Figure 25. Comparison of concentration verses HRT driven changes on net TP balance assuming 100% particle trapping. Concentrations include siphon data, and stream medians multiplied by a factor of 0.5, 1 and 2, while HRT is varied between 10 and 100 days. The color scale is for Net TP Balance and applies to panels A, B, and C.

Across scenarios using what we consider the most realistic assumptions for the field sites monitored in this study, net P retention was approximately 0.1 g P m^{-2} $year^{-1}$ (1 lb. P $acre^{-1}$ yr^{-1}) (Figure 25). Very few scenarios resulted in net P export, suggesting that the wetlands investigated in this study are generally P sinks on the landscape. Figure 26 shows that across all model simulations we ran that were forced by stream concentrations, TP retention efficiency [= ((TP in – TP out) / TP in)*100%] ranged from –54 to 95%, with a mean/median across all site-scenario combinations of 38%, which happens to be very close to the value used by Singh et al. (2019) of 40% to model P load reduction from wetland restoration in the Lake Champlain Basin. TP retention efficiency was substantially higher when we assumed 100% particle trapping (mean = 55%), verses when we modeled particle settling (mean = 23%). However, wetlands for which near 100% particle trapping is likely to occur, such as at the Prindle Road site, likely receive lower sediment loads than ephemeral floodplain wetlands where settling velocity limits sediment particle trapping. To contextualize our TP retention efficiency results, we show the range predicted by our modeling exercise in this study alongside literature values for different wetland types presented by Land et al. (2016) in Figure 27.

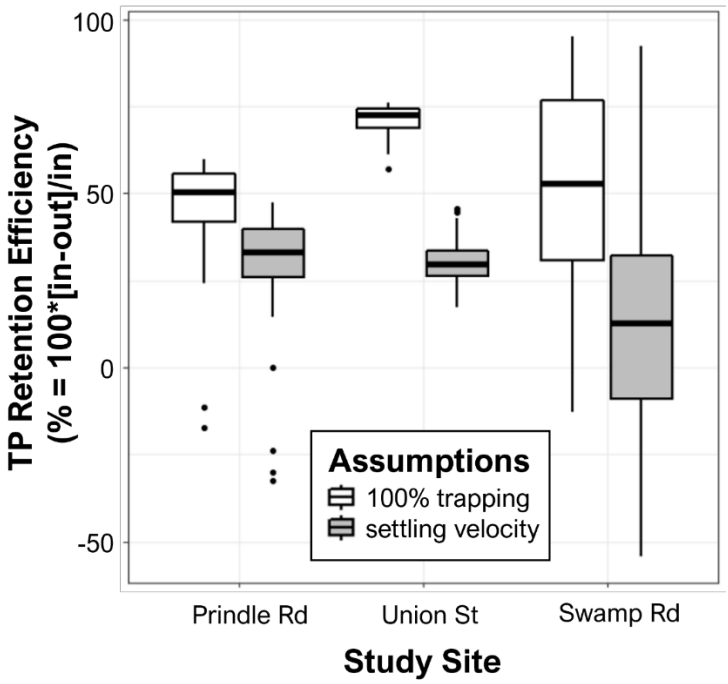

Figure 26. Box and whisker plot of TP retention efficiency (%) for all simulations of stream concentrations entering wetland plots, grey boxes indicate simulations where sedimentation is via settling velocity, white boxes indicate simulations where 100% particle trapping is assumed.

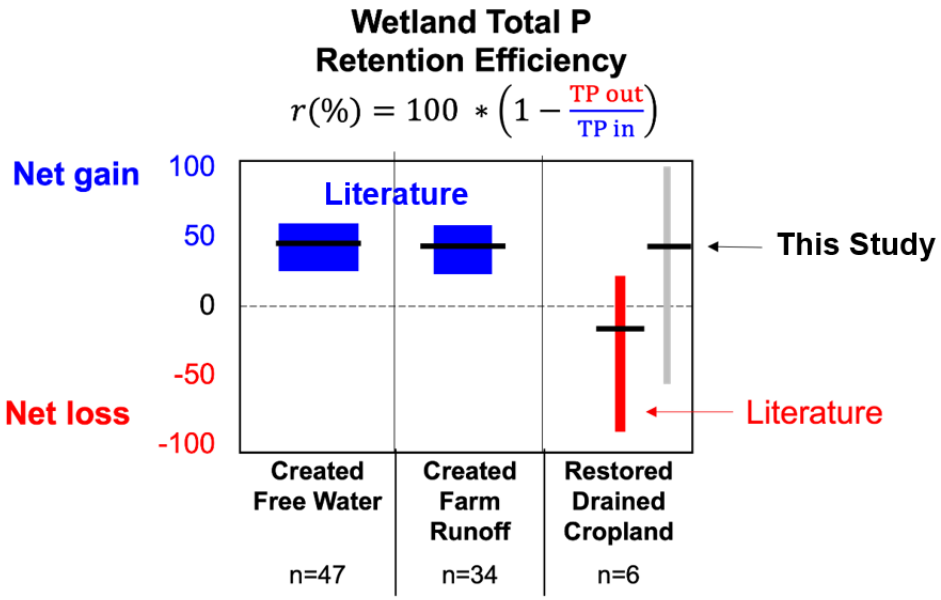

Figure 27. Comparison of wetland total phosphorus (TP) retention efficiency (%) estimates in this study with existing literature for different wetland types. Literature estimates in blue and red come from Land et al. (2016). Note that n = 3 for this study. Vertical bar = range, width of vertical bar is proportional to n, black horizontal line = median.

Our findings highlight the importance of considering both particulate and dissolved P in P mass balances for restored wetlands and other green infrastructure. Basing estimates of P retention on P

deposition (i.e., particle trapping) alone will likely lead to overestimates of net P retention in mass per area per year. While the TP balance in my simulations tended to be positive, the balance of bioavailable SRP [=DIP] tended to be negative (Figure 28). Net retention of SRP [= ((DIP in – DIP out) / DIP in)*100%] was negative on average (mean = -23%), indicating that there was net release of SRP from the wetlands. The trend of decreasing SRP retention efficiency illustrates how legacy P and watershed P buffering capacity could potentially frustrate efforts to reduce P loading. As upstream concentrations decrease because of adoption of best management practices, the stream/wetland/floodplain sediments and soils effectively serve as a buffer and release more SRP in an attempt to come into equilibrium with influent waters. In aggregate, this P buffering capacity causes watersheds to resist change in SRP concentrations while legacy P stocks slowly deplete, creating a time lag between actions (adoption of BMPs) and results (reduced SRP concentrations) (Goyette et al., 2018).

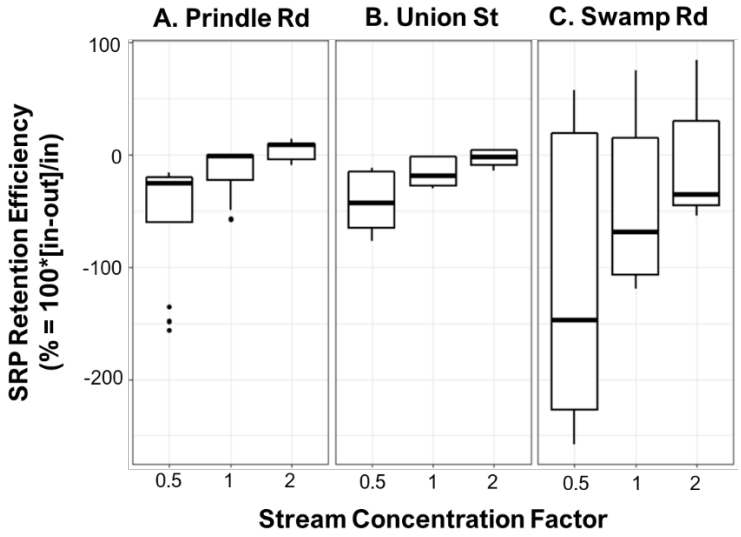

Figure 28. Box and whisker plots of SRP retention efficiency, grouped by site and stream concentration factor, for all simulations forced by stream concentrations.

It is also important to consider the foregone agricultural P loading for parcels converted from agriculture to wetlands. P losses from fields producing corn silage or hay and having clay soils representative of the LCB have been estimated to be approximately 0.1 g P m^{-2} $year^{-1}$ (1 lb P $acre^{-1}$ yr^{-1}) for surface runoff and approximately 0.1 g P m^{-2} $year^{-1}$ (1 lb P $acre^{-1}$ yr^{-1}) for subsurface runoff if a field is drained (Joshua Faulkner, UVM Extension, personal communication). If we assume only surface runoff would have occurred at low elevation sites studied in this project that were restored back to wetlands, the overall benefit of switching from farming to wetland, including foregone P loading from agriculture and wetland P capture, would be approximately 0.2 g P m^{-2} $year^{-1}$ (2 lbs P $acre^{-1}$ yr^{-1}) (double than if we only consider wetland function today). If a site that currently functions similarly to the wetlands evaluated in this project also formerly included subsurface drainage, then the overall benefit could be around 0.3 g P m^{-2} $year^{-1}$ (3 lbs P $acre^{-1}$ yr^{-1}).

It is important to note that dissolved oxygen and periphyton dynamics are not currently represented in the model. Periphyton uptake of SRP from the water column during warm periods could potentially limit SRP movement from soils to the water column during inundation. The model could therefore be slightly overestimating SRP release during periods of high periphyton productivity. On the other hand, oxygen depletion of surface waters could promote higher equilibrium SRP concentrations due to dissolution of Fe and associated P (as seen in our intact core incubations). The model may therefore be underestimating SRP release during summer periods of high soil mineralization rates and soil oxygen demand, and in winter periods of low primary productivity and ice inhibition of oxygen diffusion. It is possible that the effects of primary production, decomposition, and soil oxygen depletion on TP/SRP balance effectively cancel out and that by omitting these counteracting processes we are approximating average conditions. However, at present it is not clear which mechanisms have a greater effect on net TP and SRP balances. Future versions of the model could incorporate dissolved oxygen and periphyton dynamics and evaluate their relative importance for net P retention and net SRP retention. A more quantitative assessment of model sensitivity and uncertainty should also be conducted to help guide the interpretation of the net P retention estimates produced by the model and to establish the threshold for changes in P loads to be considered significant (Hantush & Chaudhary, 2014; Chaudhary & Hantush, 2017).

In this project, we have demonstrated the use of the model using detailed ecosystem and hydroclimatic inputs for three field sites, but the model is flexible. With a few slight modifications it would capable simulating average hydroclimatic conditions across a range of soils with relatively few inputs. In the future when modeling Vermont soils with unknown equilibrium SRP concentration, data from laboratory intact core incubations conducted as part of this LCBP project and for other work undertaken by project team members can be used to model SRP from known values of P Saturation Ratio (PSR) and soil P storage capacity (SPSC). Furthermore, PSR and SPSC could likely be modeled from geospatial soil and land use datasets in lieu of site data (Cohen et al., 2007; Kang et al., 2009; Welikhe et al., 2020). Once equilibrium SRP can be estimated across a wide range of sites, a number of possible model applications arise. For example, it would also be possible to test how different efforts to restore wetland ecosystems via establishment of woody vegetation, biomass harvest, or ditch plugging could affect long-term net P retention for a given set of soil and hydrologic conditions. This could provide useful information in efforts to determine which management actions would be most appropriate for the many thousands of potential wetland restoration sites in Vermont (VT DEC, 2018).

6. Conclusions

Very few past studies have determined net P retention for restored riparian wetland ecosystems on formerly farmed land (Land et al., 2016), none of which occurred in the Northeast U.S. In this project, we were able to make detailed measurements of P deposition in three riparian wetland systems in the LCB subjected to multiple flood pulses, including variation in P deposition with elevation, correction for internal particulate P cycling (e.g., plant litter), and clarification of mineral versus organic matter. When comparing our findings to those in Diehl et al. (2021), the three sites that we monitored appear to be on the lower end of the spectrum for floodplain P deposition that is possible in the LCB (up to approximately 1 g P m^{-2} yr^{-1}).

Our findings also confirm the importance of considering both particulate and dissolved P in P mass balances for restored wetlands. Basing estimates of P retention on P deposition (i.e., particle trapping) alone will likely lead to overestimates of net P retention in mass per area per year. A sizable fraction of wetland soil P at the sites included in this study (up to approximately one half depending on site and plot) was associated with forms having potential to eventually become bioavailable. Release of SRP (i.e., DIP) from wetland soils during flood pulses will likely vary based on soil properties. Our three field sites fall at the low end (Union Street) and in the middle range (Prindle Road and Swamp Road) of SRP release within a larger group of LCB soils analyzed by the project team using intact soil core incubations in the laboratory across multiple projects.

A large amount of field data were collected at our three field sites to enable modeling of riparian wetland P cycling using a newly coded Wetland P Model in R. The model includes multiple P fluxes and transformations, and yields net P balance results that incorporate particulate and dissolved P fluxes. Across model scenarios using what we consider the most realistic assumptions, net P retention was approximately 0.1 g P m^{-2} $year^{-1}$ (1 lb P $acre^{-1}$ yr^{-1}). Very few scenarios resulted in net P export, suggesting that the wetlands investigated in this study are generally P sinks on the landscape. If former agricultural P loading is also factored in, the overall net P load decrease could rise to 0.2 or 0.3 g P m^{-2} $year^{-1}$ (2 or 3 lbs P $acre^{-1}$ yr^{-1}), depending on the site's former use and drainage.

The retention efficiencies for TP and SRP (i.e., DIP) were on average +38% (net gain) and -23% (net loss), respectively, but varied widely across all site-scenario combinations, illustrating the importance of site factors (e.g., equilibrium P concentration for soils), hydrology, and influent TSS and TP concentrations. These results highlight the potential TP load reduction benefits associated with the restoration of floodplain wetlands. However, they also suggest that release of legacy P in soluble forms can complicate watershed management efforts. As upstream TSS and P concentrations decrease because of adoption of best management practices, the stream/wetland/floodplain sediments and soils effectively serve as a buffer and release more SRP to come into equilibrium with influent waters. In aggregate, this P buffering capacity causes watersheds to resist change in SRP concentrations while legacy P stocks slowly deplete, creating a time lag between actions (adoption of BMPs) and results (reduced P concentrations) (Goyette et al., 2018).

In conclusion, this project has addressed important gaps in understanding the extent to which restored riparian wetlands will serve as a P sink in the LCB, corresponding to Strategies I.A.1.c (Increase understanding of factors affecting BMP performance and efficiency) and I.C.1.b (Fund programs to protect or enhance river corridors for nutrient reduction and flood resilience) within the LCBP 2017 Opportunities for Action. Outputs from this project can aid the refinement of wetland restoration efforts, resulting in efficient use of state and non-profit resources to reduce P loading to Lake Champlain.

7. References

Albert, C., Spangenberg, J. H., and Schröter, B. (2017). Nature-based solutions: criteria. Nature, 543(7645), 315-315

Arrowwood Environmental and Fitzgerald Environmental Associates (2017), http://arrowwoodvt.com/rcppmodelsites/; website Accessed Nov 2017

Augustin, I. C. (2021). Hydrologic Modeling of a Small Wetland Complex to Inform Estimates of Phosphorus Retention. Honors Thesis. University of Vermont. https://scholarworks.uvm.edu/hcoltheses/381/

Bedford, B. L., Walbridge, M. R., & Aldous, A. (1999). Patterns in Nutrient Availability and Plant Diversity of Temperate North American. Ecology, 80(7), 2151–2169. https://doi.org/10.2307/176900

Bolster, C. H., & Hornberger, G. M. (2007). On the Use of Linearized Langmuir Equations. Soil Science Society of America Journal, 71(6), 1796–1806. https://doi.org/10.2136/sssaj2006.0304

Bouyoucos, G. J. (1962). Hydrometer method improved for making particle size analyses of soils. Agronomy, 54(5), 464–465.

Callaway, J. C., Cahoon, D. R., Lynch, J. C., DeLaune, R. D., Reddy, K. R., Richardson, C. J., & Megonigal, J. P. (2013). The Surface Elevation Table–Marker Horizon Method for Measuring Wetland Accretion and Elevation Dynamics. (January). https://doi.org/10.2136/sssabookser10.c46

Chaudhary, A., & Hantush, M. M. (2017). Bayesian Monte Carlo and maximum likelihood approach for uncertainty estimation and risk management: Application to lake oxygen recovery model. Water Research, 108, 301–311. https://doi.org/10.1016/j.watres.2016.11.012

Chimney, M. J., & Pietro, K. C. (2006). Decomposition of macrophyte litter in a subtropical constructed wetland in south Florida (USA). Ecological Engineering, 27(4), 301–321. https://doi.org/10.1016/j.ecoleng.2006.05.016

Cohen, M. J., Paris, J., & Clark, M. W. (2007). P-sorption capacity estimation in southeastern USA wetland soils using visible/near infrared (VNIR) reflectance spectroscopy. Wetlands, 27(4), 1098–1111. https://doi.org/10.1672/0277-5212(2007)27[1098:PCEISU]2.0.CO;2

Courchesne, F., & Turmel, M. C. (2008). Extractable Al, Fe, Mn, and Si. In M. Carter & E. Gregorich (Eds.), Soil Sampling and Methods of Analysis (Second Edi, pp. 307–315). CRC Press Taylor and Francis Group.

Cronk, J. K., & Fennessy, M. S. (2001). WETLAND PLANTS: biology and ecology (1st ed.). Boca Raton, FL: CRC Press.

Currie, S. J., Vanzomeren, C. M., & Berkowitz, J. F. (2017). Utilizing Wetlands for Phosphorus Reduction in Great Lakes Watersheds : A Review of Available Literature Examining Soil Properties and Phosphorus Removal Efficiency. U.S. Army Engineer Research and Development Center (October 2017). EDRC/EL SR-17-4

D'Angelo, E., Crutchfield, J., & Vandiviere, M. (2001). Rapid, Sensitive, Microscale Determination of Phosphate in Water and Soil. Journal of Environment Quality, 30(6), 2206. https://doi.org/10.2134/jeq2001.2206

Day, P. R. (1965). Hydrometer method of particle size analysis. Methods of soil analysis. Agronomy, 9, 562–566.

Diehl, T. H. (2007). A Modified Siphon Sampler for Shallow Water. USGS.

Diehl, R.M., B.C. Wemple, K.L. Underwood, D. Ross. 2021. "Evaluating floodplain potential for sediment and phosphorus deposition: Development of a framework to assist in Lake Champlain Basin planning". Report to the Lake Champlain Basin Program, June 2021.

Dudley, R.W., Hodgkins, G.A., McHale, M.R., Kolian, M.J., Renard, B. (2017). Trends in snowmelt-related streamflow timing in the conterminous United States. *J. Hydrology*, 547, 208-221.

Dunne, E. J., Smith, J., Perkins, D. B., Clark, M. W., Jawitz, J. W., & Reddy, K. R. (2007). Phosphorus storages in historically isolated wetland ecosystems and surrounding pasture uplands. Ecological Engineering, 31(1), 16–28. https://doi.org/10.1016/j.ecoleng.2007.05.004

Faulkner, J. W. (n.d.). Personal Communication. Email: Wednesday, September 29, 2021 3:01 PM.

Fisher, J. and Acreman, M.C. (2004). Wetland nutrient removal: a review of the evidence. Hydrology and Earth System Sciences, 8(4), 673-685

Fisher, M. M., & Reddy, K. R. (2001). Phosphorus flux from wetland soils affected by long-term nutrient loading. Journal of Environmental Quality, 30(1), 261–271. https://doi.org/10.2134/jeq2001.301261x

Freeman, C., Ostle, N., & Kang, H. (2001). An enzymic "latch" on a global carbon store. Nature, 409(6817), 149. https://doi.org/10.1038/35051650

Goyette, J.-O., Bennett, E. M., & Maranger, R. (2018). Low buffering capacity and slow recovery of anthropogenic phosphorus pollution in watersheds. Nature Geoscience. https://doi.org/10.1038/s41561-018-0238-x

Graetz, D. A., & Nair, V. D. (2009). Phosphorus Sorption Isotherm Determination. In G. M. Kovar, John L. Pierzynski (Ed.), Methods of Phosphorus Analysis for Soils, Sediments, Residuals, and Waters (2nd ed., pp. 33–38). Retrieved from http://www.sera17.ext.vt.edu/Documents/P_Methods2ndEdition2009.pdf

Gu, S., Gruau, G., Malique, F., Dupas, R., Petitjean, P., & Gascuel-Odoux, C. (2018). Drying/rewetting cycles stimulate release of colloidal-bound phosphorus in riparian soils. Geoderma. https://doi.org/10.1016/j.geoderma.2018.01.015

Guilbert, J., Beckage, B., Winter, J. M., Horton, R. M., Perkins, T., & Bomblies, A. (2014). Impacts of projected climate change over the Lake Champlain basin in Vermont. Journal of Applied Meteorology and Climatology, 53(8), 1861–1875. https://doi.org/10.1175/JAMC-D-13-0338.1

Hantush, M. M., Kalin, L., Isik, S., & Yucekaya, A. (2013). Nutrient Dynamics in Flooded Wetlands. I: Model Development. Journal of Hydrologic Engineering, 18(12), 1709–1723. https://doi.org/10.1061/(ASCE)HE.1943-5584.0000741

Hantush, Mohamed M., & Chaudhary, A. (2014). Bayesian framework for water quality model uncertainty estimation and risk management. Journal of Hydrologic Engineering, 19(9). https://doi.org/10.1061/(ASCE)HE.1943-5584.0000900

Heim, R., & A. Sanchez-Lugo. 2021. Vermont. U.S. Drought Monitor. https://droughtmonitor.unl.edu/CurrentMap/StateDroughtMonitor.aspx?VT

Hodgkins, G. A., and R. W. Dudley (2006), Changes in the timing of winter–spring streamflows in eastern North America, 1913–2002, Geophys. Res. Lett., 33, L06402, doi:10.1029/2005GL025593.

Hoffmann, C. C., Kjaergaard, C., Uusi-Kämppä, J., Hansen, H. C. B., & Kronvang, B. (2009). Phosphorus Retention in Riparian Buffers: Review of Their Efficiency. Journal of Environment Quality, 38(5), 1942. https://doi.org/10.2134/jeq2008.0087

Jones, C. N., Scott, D. T., Guth, C., Hester, E. T., & Hession, W. C. (2015). Seasonal variation in floodplain biogeochemical processing in a restored headwater stream. Environmental Science & Technology, 49(22), 13190-13198

Kalin, L., & Hantush, M. M. (2017). Special issue on advances in wetland hydrology and water quality processes modeling. Journal of Hydrologic Engineering, 22(1), 2015–2016. https://doi.org/10.1061/(ASCE)HE.1943-5584.0001483

Kang, J., Hesterberg, D., & Osmond, D. L. (2009). Soil Organic Matter Effects on Phosphorus Sorption: A Path Analysis. Soil Science Society of America Journal, 73(2), 360–366. https://doi.org/10.2136/sssaj2008.0113

Kiedrzyńska, E., Wagner, I., & Zalewski, M. (2008). Quantification of phosphorus retention efficiency by floodplain vegetation and a management strategy for a eutrophic reservoir restoration. Ecological Engineering, 33(1), 15–25. https://doi.org/10.1016/j.ecoleng.2007.10.010

Land, M., Granéli, W., Grimvall, A., Hoffmann, C. C., Mitsch, W. J., Tonderski, K. S., & Verhoeven, J. T. A. (2016). How effective are created or restored freshwater wetlands for nitrogen and phosphorus removal? A systematic review. Environmental Evidence, 5(1), 1–26. https://doi.org/10.1186/s13750-016-0060-0

Lent, R.M. (1997). Hydrologic indices for nontidal wetlands. Wetlands, 17(1), 19-30

Levy, E. T., & Schlesinger, W. H. (1999). A comparison of fractionation methods for forms of phosphorus in soils. Biogeochemistry, 47(1), 25–38. https://doi.org/10.1007/bf00993095

Marois, D. E., & Mitsch, W. J. (2016). Modeling phosphorus retention at low concentrations in Florida Everglades mesocosms. Ecological Modelling, 319, 42–62. https://doi.org/10.1016/j.ecolmodel.2015.09.024

McMillan, S. K., & Noe, G. B. (2017). Increasing floodplain connectivity through urban stream restoration increases nutrient and sediment retention. Ecological Engineering, 108(March), 284–295. https://doi.org/10.1016/j.ecoleng.2017.08.006

Mitsch, W. J., Zhang, L., Stefanik, K. C., Nahlik, A. M., Anderson, C. J., Bernal, B., ... and Song, K. (2012). Creating wetlands: primary succession, water quality changes, and self-design over 15 years. Bioscience, 62(3), 237-250

Morris, J. T., Barber, D. C., Callaway, J. C., Chambers, R., Hagen, S. C., Hopkinson, C. S., … Wigand, C. (2016). Contributions of organic and inorganic matter to sediment volume and accretion in tidal wetlands at steady state. Earth's Future, 4(4), 110–121.

Murphy, J., & Riley, J. P. (1962). A modified single solution method for the determination of phosphate in natural waters. Analytica Chimica Acta, 27(C), 31–36. https://doi.org/10.1016/S0003-2670(00)88444-5

Nair, V. D., & Harris, W. G. (2004). A capacity factor as an alternative to soil test phosphorus in phosphorus risk assessment. New Zealand Journal of Agricultural Research, 47(4), 491–497. https://doi.org/10.1080/00288233.2004.9513616

O'Dell, J. W. (1993). Method 365.1, Determination of Phosphorus By Semi-Automated Colorimetry. Epa, (August), 1–15.

Patton, C. J., & Kryskalla, J. R. (2003). Methods of Analysis by the U.S. Geological Survey National Water Quality Laboratory—Evaluation of Alkaline Persulfate Digestion as an Alternative to Kjeldahl Digestion for Determination of Total and Dissolved Nitrogen and Phosphorus in Water. In Water-Resources Investigations Report (Vol. 03–4174). Denver, CO.

Reddy, K. R., Wang, Y., DeBusk, W. F., Fisher, M. M., & Newman, S. (1998). Forms of Soil Phosphorus in Selected Hydrologic Units of the Florida Everglades. Soil Science Society of America Journal, 62(4), 1134–1147. https://doi.org/10.2136/sssaj1998.03615995006200040039x

Reddy, K. R., Kadlec, R. H., Flaig, E., and Gale, P. M. (1999). Phosphorus retention in streams and wetlands: a review. Critical reviews in environmental science and technology, 29(1), 83-146

Reddy, K. R., Clark, M. W., DeLaune, R. D., & Kongchum, M. (2013). Physicochemical Characterization of Wetland Soils. In SSSA Book Series SV - 10. Methods in Biogeochemistry of Wetlands (pp. 41–53). https://doi.org/10.2136/sssabookser10.c3

Reddy, K. R., & Delaune, R. D. (2008). Biogeochemistry of wetlands. CRC Press.

Richardson, C. J., & Reddy, K. R. (2013). Methods for Soil Phosphorus Characterization and Analysis of Wetland Soils. In SSSA Book Series SV - 10. Methods in Biogeochemistry of Wetlands (pp. 603–638). https://doi.org/10.2136/sssabookser10.c32

Ries, K. G. I., Newson, J. K., Smith, M. J., Guthrie, J. D., Steeves, P. A., Haluska, T. L., et al. (2017). StreamStats, Version 4.

Ringuet, S., Sassano, L., & Johnson, Z. I. (2011). A suite of microplate reader-based colorimetric methods to quantify ammonium, nitrate, orthophosphate and silicate concentrations for aquatic nutrient monitoring. J. Environ. Monit., 13(2), 370–376. https://doi.org/10.1039/C0EM00290A

Roy, E. D., Nguyen, N. T., Bargu, S., & White, J. R. (2012). Internal loading of phosphorus from sediments of Lake Pontchartrain (Louisiana, USA) with implications for eutrophication. Hydrobiologia, 684(1), 69–82. https://doi.org/10.1007/s10750-011-0969-9

Roy, E. D., Smith, E. A., Bargu, S., & White, J. R. (2016). Will Mississippi River diversions designed for coastal restoration cause harmful algal blooms? Ecological Engineering, 91, 350–364. https://doi.org/10.1016/j.ecoleng.2016.02.030

Roy, E. D., Nguyen, N. T., & White, J. R. (2017). Changes in estuarine sediment phosphorus fractions during a large-scale Mississippi River diversion. Science of the Total Environment, 609, 1248–1257. https://doi.org/10.1016/j.scitotenv.2017.07.224

Schönbrunner, I. M., Preiner, S., & Hein, T. (2012). Impact of drying and re-flooding of sediment on phosphorus dynamics of river-floodplain systems. Science of the Total Environment, 432, 329–337. https://doi.org/10.1016/j.scitotenv.2012.06.025

Sigua, G. C., Coleman, S. W., & Albano, J. (2009). Beef cattle pasture to wetland reconversion: Impact on soil organic carbon and phosphorus dynamics. Ecological Engineering, 35(8), 1231–1236. https://doi.org/10.1016/j.ecoleng.2009.05.004

Singh, N., Gourevitch, J. D., Wemple, B. C., Watson, K. B., Rizzo, D. M., Polasky, S., & Ricketts, T. (2019). Optimizing wetland restoration to improve water quality at a regional scale. Environmental Research Letters. https://doi.org/10.1088/1748-9326/ab1827

Soil Science Division Staff. (2017). Soil Survey Manual, USDA Handbook 18. (18), 639.

Surridge, B. W. J., Heathwaite, A. L., & Baird, A. J. (2012). Phosphorus mobilisation and transport within a long-restored floodplain wetland. Ecological Engineering, 44, 348–359. https://doi.org/10.1016/j.ecoleng.2012.02.009

Trueheart, M.E., "Simulating hydraulic interdependence between bridges along a river corridor under transient flood conditions" (2019). Graduate College Dissertations and Theses. 1042. https://scholarworks.uvm.edu/graddis/1042

Trueheart, M. E., Dewoolkar, M. M., Rizzo, D. M., Huston, D., & Bomblies, A. (2020). Simulating hydraulic interdependence between bridges along a river corridor under transient flood conditions. Science of the Total Environment, 699, 134046. https://doi.org/10.1016/j.scitotenv.2019.134046

US EPA. (2016). Phosphorus TMDL for Vermont segments of Lake Champlain.

VCGI (Vermont Center for Geographic Information). 2018. Quality Level 2 Lidar Hydro-Flattened Digital Elevation Model (DEMHF) data from the 3D Elevation Program (3DEP). https://maps.vcgi.vermont.gov/gisdata/metadata/ElevationDEM_DEMHF0p7M2017.htm

VT DEC. (2018). RCPP wetland restoration site prioritization project map introduction. Vermont Department of Environmental Conservation Watershed Management Division.

Wang, H., Appan, A., & Gulliver, J. S. (2003). Modeling of phosphorus dynamics in aquatic sediments: I - Model development. Water Research. https://doi.org/10.1016/S0043-1354(03)00304-X

Wang, N., and Mitsch, W. J. (2000). A detailed ecosystem model of phosphorus dynamics in created riparian wetlands. Ecological Modelling, 126(2), 101-130

Watson, K. B., Ricketts, T., Galford, G., Polasky, S., & O'Niel-Dunne, J. (2016). Quantifying flood mitigation services: The economic value of Otter Creek wetlands and floodplains to Middlebury, VT. Ecological Economics, 130, 16–24. https://doi.org/10.1016/j.ecolecon.2016.05.015

Welikhe, P., Brouder, S. M., Volenec, J. J., Gitau, M., & Turco, R. F. (2020). Development of phosphorus sorption capacity-based environmental indices for tile-drained systems. Journal of Environmental Quality, 49(2), 378–391. https://doi.org/10.1002/jeq2.20044

8. Appendices

Appendix A – Model Documentation
Appendix B – Flow Analysis
Appendix C – Model Calibration
Appendix D – Project data, photos, and R programming code